An endothelial SOX18-mevalonate pathway axis enables repurposing of statins for infantile hemangioma

Annegret Holm[1,10], Matthew S. Graus[2], Jill Wylie-Sears[1], Luke Borgelt[1], Jerry Wei Heng Tan[1,9], Sana Nasim[1], Long Chung[2], Ashish Jain[3], Mingwei Sung[3], Liang Sun[3], Pascal Brouillard[4], Ramrada Lekwuttikarn[5], Harry Kozakewich[6], Jacob Yanfei Qi[2], Joyce C. Teng[5], John B. Mulliken[7], Miikka Vikkula[4,8], Mathias Francois[2] and Joyce Bischoff[1*]

Affiliations:

[1] Vascular Biology Program, Department of Surgery, Boston Children's Hospital, Harvard Medical School, Boston, MA, United States.
[2] Centenary Institute, The University of Sydney, Royal Prince Alfred Hospital, Sydney, NSW, Australia
[3] Research Computing, Information Technology, Boston Children's Hospital, Boston, United States.
[4] Human Molecular Genetics, de Duve Institute, University of Louvain, Brussels, Belgium; VASCERN-VASCA European Reference Center.
[5] Department of Dermatology, Lucile Packard Children's Hospital at the Stanford University School of Medicine, Palo Alto, California.
[6] Department of Pathology, Boston Children's Hospital, Harvard Medical School, Boston, MA, United States.
[7] Department of Plastic and Oral Surgery, Boston Children's Hospital; Department of Surgery, Harvard Medical School, Boston, United States.
[8] WELBIO department, WEL Research Institute, Wavre, Belgium.
[9] School of Biological Sciences, Nanyang Technological University, Singapore, Singapore
[10] Division of Pediatric Hematology and Oncology, University Hospital of Freiburg, Germany; VASCERN-VASCA European Reference Center.

*Address correspondence to:

Joyce Bischoff, PhD
Karp Family Research Laboratories 12.212
Boston Children's Hospital
300 Longwood Ave.
Boston, MA 02115
Phone: 617-919-2192
Email: joyce.bischoff@childrens.harvard.edu

ABSTRACT:

Infantile hemangioma (IH) is the most common tumor in children and a paradigm for pathological vasculogenesis, angiogenesis and regression. Propranolol is the mainstay of treatment for IH. It inhibits hemangioma vessel formation via a β-adrenergic receptor independent off-target effect of its R(+) enantiomer on the endothelial specific transcription factor sex-determining region Y (SRY) box transcription factor 18 (SOX18). Transcriptomic profiling of patient-derived hemangioma stem cells uncovered the mevalonate pathway (MVP) as a target of R(+) propranolol. Loss of SOX18 function confirmed R(+) propranolol mode of action on the MVP. Functional validation in preclinical IH models revealed that statins - targeting the MVP - are potent inhibitors of hemangioma vessel formation. We propose a novel SOX18-MVP-axis as a central regulator of IH pathogenesis and suggest statin repurposing to treat IH. Our findings reveal novel pleiotropic effects of beta-blockers and statins acting on the SOX18-MVP axis to disable an endothelial specific program in IH, which may impact other scenarios involving pathological vasculogenesis and angiogenesis.

52 **INTRODUCTION:**

53 Infantile hemangioma (IH) is a common benign vascular tumor of infancy with an incidence of 2-10%. It
54 predominantly occurs in female and premature infants of European descent. IH arises postnatally at 3-7
55 weeks of age and grows rapidly during the proliferating phase, which can continue for 12 months on
56 average. A spontaneous and gradual involuting phase follows spanning 2-7 years. A subtype of IH - often
57 involving the oral mucosa - do not undergo complete involution and may regrow after treatment
58 discontinuation. For most children, IH poses no serious risk; however, 10-15% of lesions require
59 treatment to prevent sequelae such as disfigurement and functional impairment including vision loss
60 and airway obstruction, consumptive hypothyroidism, and high-output cardiac failure (1). Propranolol
61 was discovered serendipitously to be effective for IH. It is currently the only FDA-approved drug for IH,
62 based on a randomized controlled clinical trial (2). Despite its successful repurposing for IH, propranolol
63 is associated with beta-adrenergic side effects including hypotension, bradycardia, peripheral
64 vasospasm, hypoglycemia and seizures, bronchospasm, slowed weight gain, diarrhea, agitation, sleep
65 disturbance, and potentially adverse neurocognitive outcomes (2-5). The complete response rate to
66 propranolol is reported to be 60%; a subset of IH regrow after treatment is discontinued (2). These
67 safety and efficacy concerns underscore the need for additional treatment options for patients with IH.
68

69 It is firmly established that propranolol acts as a non-selective antagonist of the G protein-coupled β1-
70 and β2-adrenergic receptors (GPCR). Propranolol consists of an equimolar (1:1) mixture of S(-) and R(+)
71 enantiomers. The S(-) enantiomer is a potent antagonist of β1 and β2-adrenergic receptors, while the
72 R(+) enantiomer is largely devoid of beta-blocker activity (6). This provided an opportunity to identify a
73 novel R(+) propranolol-dependent pathway in hemangioma stem cells (HemSC). HemSC are isolated
74 from proliferating phase patient IH specimens and recapitulate hemangiogenesis in nude mice (7). R(+)
75 propranolol inhibits HemSC endothelial differentiation in vitro and HemSC vasculogenesis in a pre-
76 clinical model (8, 9). Furthermore, we established that R(+) propranolol interferes with the activity of the
77 transcription factor (TF) SRY (sex-determining region Y) HMG box-containing 18 (SOX18).
78 Pharmacological interference has also been observed with Sm4 - a small molecule inhibitor of SOX18 -
79 further validating the role of this molecular target in IH (8, 9). These findings have led to the repurposing
80 of propranolol in patients with hypotrichosis-lymphedema-telangiectasia-renal defect syndrome (HLTRS)
81 - a rare vascular disease caused by a dominant-negative truncating mutation in SOX18 (10). Together,
82 these observations provided evidence for the pharmaco-genetic interaction between SOX18 and
83 propranolol in human disease (8). In summary, we have identified a SOX18-dependent inhibition of

84 HemSC endothelial differentiation and vessel formation in vivo as the molecular basis of propranolol-
85 mediated inhibition of IH.
86
87 SOX18 is a master regulator of vascular development and endothelial specification and is expressed in
88 nascent differentiating blood and lymphatic endothelium as well as in endothelial progenitor cells in
89 adults (11). It plays fundamental roles in arterial specification (12), lymphangiogenesis (13) and tumor
90 angiogenesis (14). Because of its known role during embryogenesis, this prompted us to investigate the
91 molecular basis of its pharmacological blockade in the context of HemSC endothelial differentiation.
92
93 To elucidate the functional role of SOX18 in IH vasculogenesis, we set out to identify genes whose
94 expression in differentiating HemSC is altered by R(+) propranolol. We discovered that R(+) propranolol
95 coordinately downregulates transcripts encoding enzymes in the mevalonate pathway (MVP). The MVP
96 is central to cholesterol and isoprenoid biosynthesis and is controlled by the rate-limiting enzyme 3-
97 hydroxy-3-methylglutaryl-CoA reductase A (HMGCR) (15), which produces mevalonate. Additional
98 regulators are the transcription factor sterol regulatory element binding protein-2 (SREBP2) that induces
99 expression of MVP genes (16) and the ATP-binding cassette transporter A1 (ABCA1) that acts as a
100 negative regulator of SREBP2 by facilitating retrograde transport of cholesterol from the plasma
101 membrane to the endoplasmic reticulum (ER) (17). Statins, competitive HMGCR inhibitors, are widely
102 prescribed to reduce low-density-lipoprotein cholesterol in patients at risk for cardiovascular disease
103 (18). Pleiotropic activities of statins beyond the lipid-lowering effect have been established (19-21).
104 Accumulating evidence suggests a role for statins in epigenetic modifications in a cardiovascular disease
105 and an oncology context (22-24). Here, we uncover a novel molecular relationship between an
106 endothelial specific TF and the MVP. We show that R(+) propranolol causes a SOX18-mediated
107 downregulation of MVP genes in HemSC during their endothelial differentiation. Blocking the MVP with
108 statins inhibits endothelial differentiation and vessel formation, suggesting that statins could be
109 repurposed to safely treat the vascular overgrowth in IH.
110

111 **RESULTS:**

112 ***R(+) propranolol globally reduces transcript levels of MVP genes in patient-derived HemSC undergoing***
113 ***endothelial differentiation.***

114 To identify the downstream targets of R(+) propranolol in HemSC to hemangioma endothelial cell
115 (HemEC) differentiation in a non-biased way, we performed bulk RNA sequencing of HemSC isolated
116 from 6 different IH specimens. Table 1 provides an overview of patient samples used in respective
117 experiments. The HemSC were induced to undergo endothelial differentiation for 6 days and then
118 treated with or without R(+) propranolol (20uM) for 2 hours (Supplemental Figure 1.1). The timing and
119 dosage were determined by previously observed downregulation of *NOTCH1* expression, a widely
120 known *SOX18* transcriptional target, under this treatment condition (9). HemSC at Day 4 of endothelial
121 differentiation, prior to onset of endothelial marker expression, were analyzed as well. The Kyoto
122 Encyclopedia of Genes and Genomes (KEGG) analysis identified steroid biosynthesis as differentially
123 affected at Day 6 (Supplemental Figure 1.2), which was confirmed by gene ontology analysis of the
124 subontology *biological processes* (8 of the top 20 processes are related to cholesterol biosynthesis)
125 (Figure 1A). Subsequent gene by gene analysis revealed R(+) propranolol treatment on Day 6
126 significantly reduced transcripts encoding several enzymes of the MVP, including the rate-limiting
127 enzyme HMGCR as well as 3-hydroxy-3-methylglutaryl-CoA synthase 1 (HMGCS1) and mevalonate
128 kinase (MVK), while few changes were seen at Day 4 (Figure 1B,C; Supplemental Table S1). The
129 significant increase in *SOX18* mRNA from Day 4 to Day 6 of differentiation is consistent with the onset of
130 MVP gene sensitivity to R(+) propranolol at Day 6 (Figure 1D). Downregulation of *HMGCS1*, *HMGCR*, and
131 *MVK* as well as upregulation of *ABCA1* - a negative regulator of SREBP2 transcriptional activity - was
132 confirmed by qPCR in cells treated with R(+) propranolol for 2 hours or for 4 days of the differentiation
133 protocol (Figure 1E). Overall, 105 genes in HemSC were differentially expressed at Day 4 versus 2482
134 genes at Day 6 of differentiation. Differential expression was defined as $\log_2$ fold change >1 and adjusted
135 p-value <0.05. The increase in differentially expressed genes at Day 6 defines a critical time window for
136 *SOX18* inhibition and therefore R(+) propranolol effect on HemSC differentiation. This concept is further
137 supported by the lack of downregulation of MVP transcripts seen in HemSC at Day 4 of differentiation,
138 prior to endothelial marker expression. RNA-Seq data will be submitted to the Gene Expression Omnibus
139 archive at the National Center for Biotechnology Information.

140

141 To further elucidate the effect of SOX18 inhibition on the MVP, we investigated SOX18-binding locations
142 in the genome using a publicly available ChIP-Seq dataset in human umbilical endothelial cells (HUVEC)

143 (25). We discovered SOX18 binding locations within the *HMGCS1* and *HMGCR* gene loci that
144 corresponded with ENCODE candidate cis-regulatory elements (Figure 2A). The RNA-Seq experiments,
145 combined with the identification of SOX18-binding sites in regulatory regions of *HMGCS1* and *HMGCR*,
146 support the ability of R(+) propranolol to interfere with SOX18 directed transcriptional regulation of
147 critical genes in or related to the MVP.
148
149 ***SOX18 activity positively regulates MVP biosynthetic output in human endothelial cells.***
150 To validate the role of SOX18 in regulating genes in the MVP, we tested whether pharmacological
151 disruption of SOX18 activity through treatment with R(+) propranolol or the known SOX18 inhibitor Sm4
152 (26) would have an effect on cholesterol biosynthesis in HUVEC. HUVEC were first cholesterol-depleted
153 by incubation with methyl beta-cyclodextrin (MBCD) and treated ±R(+) propranolol or ± Sm4 for 16
154 hours, allowing for new cholesterol synthesis, which was then measured by targeted mass
155 spectrometry. Endogenous cholesterol levels were significantly reduced in both R(+) propranolol- and
156 Sm4-treated HUVEC, consistent with SOX18-mediated downregulation of MVP gene expression (Figure
157 2B,C). Conversely, we tested the effect of an overexpressed, dominant negative version of SOX18
158 (*Ragged Opossum* (*RaOp*)) that is known to disrupt SOX18 activity (27). High expression of $SOX18^{RaOp}$
159 decreased immunofluorescent staining for HMGCS1 and HMGCR compared to low $SOX18^{RaOp}$ indicating
160 a gene dose response effect on two key MVP enzymes (Figure 2D,E; Supplemental Figure 2.1, 2.2). Taken
161 together, both experiments demonstrate that SOX18 activity positively regulates cholesterol
162 biosynthesis in an endothelial context.
163
164 ***R(+) propranolol mode of action on the MVP is mediated via a SOX18-/SREBP2-dependent mechanism.***
165 SREBP2 is the master transcriptional regulator of the MVP and is ubiquitously expressed. We postulate
166 that in HemSC undergoing endothelial differentiation, SREBP2 and SOX18 interact to co-regulate the
167 MVP. To test this idea, we analyzed the effect of R(+) propranolol on levels of the SREBP2 precursor
168 (inactive), which is anchored in the endoplasmic reticulum, and the 62kDa NH_2 basic helix loop helix
169 (bHLH) leucine zipper domain (16, 28). The 125 kDa precursor is proteolytically cleaved to release the
170 62kDa mature form when cholesterol levels drop. The mature 62kDa form of SREBP2 then translocates
171 into the nucleus to activate transcription of MVP genes. We hypothesized that R(+) propranolol
172 disruption of SOX18 would reduce 62 kDa SREBP2 in HemSC undergoing endothelial differentiation.
173 HemSC (n=4) were treated for 2 hours ± R(+) propranolol on Day 6 of VEGF-B induced endothelial
174 differentiation. Cell lysates analyzed by Western Blot (WB) showed that R(+) propranolol decreased

175 mature 62 kDa SREBP2 (Figure 3A,B). Rapid turnover of mature SREBP2 within 4 hours has been
176 previously demonstrated (29). The reduced levels of 62kDa SREBP2 upon R(+) propranolol treatment are
177 consistent with the transcriptomic findings from bulk RNA-seq and qPCR and suggest SOX18 and SREBP2
178 interact to regulate the MVP in nascent HemEC.

179 We next assessed SOX18-dependency of the R(+) propranolol mediated effects by genetic knockdown of
180 SOX18 using shRNA. We used differentiated IH-derived HemEC for this experiment because HemEC
181 express high levels of SOX18. Lentiviral knockdown of SOX18 in three different IH-derived HemEC was
182 conducted and the extent of SOX18 knockdown was verified by qPCR and WB (Supplemental Figure
183 3.1,2). HemEC with a SOX18 knockdown efficiency >70% were used. The requirement for SOX18 in R(+)-
184 mediated downregulation of MVP genes was analyzed by qPCR measurement of *HMGCS1* and *HMGCR*
185 and *MVK* in naïve HemEC and HemEC^{shSOX18}. R(+) propranolol did not reduce the mRNA levels of MVP
186 genes in HemEC^{shSOX18} (Figure 3C-E). The known SOX18 target *NOTCH1* served as a positive control for
187 R(+) propranolol (Figure 3F). In summary, the knockdown of SOX18 in HemEC abolished the R(+)
188 propranolol effect on mRNA transcript levels of *HMGCS1*, *HMGCR* and *MVK*, showing via genetic
189 disruption of SOX18 that there is a transcriptional link between SOX18 and the MVP in IH derived cells
190 (Figure 1-3).
191

192 ***Nuclear SOX18 and SREBP2 in proliferating phase and regrowing IH indicate active MVP.***

193 Based on our transcriptomic and biochemical characterization from patient-derived HemSC and HemEC,
194 we investigated the expression and localization of SOX18 and SREBP2 in patient IH histological sections
195 of different tumor phases. We stained proliferating and involuting IH tissue sections (n=10, each) from
196 specimens excised from children with IH who had not been treated with propranolol or corticosteroid
197 (or any other treatment). Immunofluorescent staining with antibodies against human SOX18 and
198 SREBP2, and with the lectin *Ulex Europaeus Agglutinin I* (UEA1), which specifically binds to human
199 endothelial cells, showed co-localization of SOX18 and SREBP2 in endothelial nuclei throughout
200 proliferating phase IH sections. Age-matched human skin (n=4), stained in parallel for comparison, was
201 devoid of SOX18. Furthermore, SOX18 was largely absent from vessels in involuting phase IH. SOX18 is
202 not routinely detected in mature, quiescent blood vessels, as it is not needed to maintain an endothelial
203 phenotype (30). We next quantified SOX18^{+}SREBP2^{+} nuclei/endothelial nuclei as a metric for active MVP.
204 SOX18^{+}/SREBP2^{+} double positive cell nuclei in involuting phase IH specimens were significantly reduced
205 compared to proliferating phase IH (Figure 4A,B,C, Supplemental Figure 4.1-3). Moreover, we analyzed
206 tissue from two patients with regrowing IH. Both patients received beta-blocker treatment during

207 infancy with notable clinical response. However, the IH regrew significantly after discontinuation of
208 treatment. Both regrowing IH specimens were positive for nuclear SOX18 and SREBP2 along the
209 endothelium. We observed histological features of proliferating IH (nuclear co-localization of SOX18 and
210 SREBP2) as well as involuting IH (enlarged vessels, connective tissue with stromal cells and adipocyte
211 islands) in the regrowing IH (Figure 4D, Supplemental Figure 4). Anti-SOX18 staining specificity was
212 verified as shown (Supplemental Figure 4.5-8). Quantification of $SOX18^{+}SREBP2^{+}$ cells/total endothelial
213 cell nuclei in regrowing IH demonstrated a similar level as seen in proliferating IH and significantly
214 increased compared to involuting IH and age-matched skin controls (Figure 4E). In summary, the nuclear
215 co-localization of SOX18 and SREBP2 in proliferating and regrowing phase IH underscores the role of the
216 MVP in IH pathogenesis and may serve as markers to predict therapy response.
217
218 ***Statins inhibit vessel formation in a xenograft model of IH.***
219 We surmised that if the MVP is critical to IH onset and progression, statins would inhibit HemSC blood
220 vessel formation in an IH preclinical model. The effect of statins on patient-derived cells has not been
221 reported before and we therefore first tested for cell toxicity and efficacy of statins on HemSC. We
222 chose to use simvastatin and atorvastatin for our preclinical model as they are commonly used statins in
223 patients, even for infants in the case of simvastatin (31). It is well established that atorvastatin is 5-10
224 times more potent than simvastatin (32). To first address toxicity, HemSC (n=3) were induced to
225 undergo endothelial differentiation until day 6 while treated with simvastatin (0.1 - 1 µM) or
226 atorvastatin (0.01 - 0.1 µM) and respective vehicle controls. Neither statin had an effect on
227 differentiating HemSC viability compared to vehicle controls (Supplemental Figure 5.1). Next, we tested
228 the effect of statins on LDL-receptor levels in HemSC as an indirect measure of their effect on the MVP.
229 Treatment with 5 µM simvastatin or 1 µM atorvastatin for 24 hours resulted in a significant upregulation
230 of LDL-R mRNA in HemSC (n=4) (Supplemental Figure 5.2), indirectly indicating efficient inhibition of
231 HMGCR in these cells.
232
233 We first tested 1 µM simvastatin and 0.1 µM atorvastatin on VEGF-B-induced HemSC endothelial
234 differentiation as described(8). Both simvastatin and atorvastatin significantly inhibited endothelial
235 differentiation as indicated by decreased expression of the EC markers CD31 and VE-Cadherin compared
236 to vehicle control (n=3). R(+) propranolol was included as a positive control (Figure 5A). We next tested
237 if statins would impact de novo vessel formation in the murine xenograft model using IH-derived HemSC
238 (n=4 different patients) (Figure 5B). Simvastatin at 10 mg/kg/day (d) (Figure 5C,D) and atorvastatin at 1

239 mg/kg/d (Supplemental Figure 5.3) both significantly inhibited human CD31+ blood vessel formation. A
240 simvastatin dose response experiment further showed that 1 mg/kg/d was sufficient to significantly
241 inhibit vessel formation (Figure 5E). Glucose levels and body weight of mice in the simvastatin dose
242 response experiment were unaffected (Figure 5F,G). The human equivalent doses corresponding to the
243 doses used in mice are shown in Supplemental Figure 5, Supplemental Table 5.1. The effective doses of
244 simvastatin and atorvastatin in Figure 5 are below effective doses used in adults and significantly below
245 the dose used in infants for Smith Lemli Opitz Syndrome (0.5 - 1 mg/kg/d simvastatin). Of note, the
246 inhibitory effect of statins was limited to HemSC de novo vessel formation and did not impact
247 angiogenic sprouting and ingrowth of surrounding murine vessels into the Matrigel implant
248 (Supplemental Figure 5.4-5). Specificity of the anti-human CD31 and anti-mouse CD31 antibodies was
249 verified (Supplemental Figure 5.6). Taken together, our data show that simvastatin and atorvastatin
250 inhibit endothelial differentiation of HemSC in vitro and vasculogenesis in a preclinical IH xenograft
251 model. This strongly suggests the MVP contributes to vascular overgrowth in IH and can be effectively
252 targeted by statins in a translational approach.

253 **DISCUSSION:**

254 In this study, we uncovered the SOX18-MVP axis as a central regulator of IH pathogenesis.
255 The R(+) enantiomer of propranolol, shown previously to disrupt SOX18 transcriptional activities,
256 downregulates expression of several genes in the MVP in a SOX18 dependent manner and reduces
257 mature SREBP2 protein, the master regulator of the MVP. R(+) propranolol or the SOX18 inhibitor Sm4
258 decreased new synthesis of cholesterol in HUVEC. We propose that SOX18 augments the transcription
259 of MVP genes to regulate cholesterol and isoprenoid biosynthesis in HemSC undergoing endothelial
260 differentiation. Of note, SOX18 levels increase over the course of HemSC to EC differentiation; this
261 corresponds to MVP sensitivity to R(+) propranolol. Furthermore, *SOX18* ChIP binding sites are present
262 in *HMGCS1* and *HMGCR*. Together, our experimental results and observations make a compelling case
263 for the involvement of the SOX18-MVP axis in the etiology of IH and suggests statins may be a new
264 therapeutic option.
265
266 Additional experiments support these novel insights. Competitive inhibition of the rate-limiting enzyme
267 of the MVP - HGMCR - with statins (simvastatin and atorvastatin) results in significantly reduced HemSC
268 blood vessel formation in mice in a dose-dependent manner with unaffected weight and glucose levels.
269 Furthermore, the numbers of angiogenic mouse blood vessels in the HemSC/Matrigel implants were
270 unaffected, indicating statins have little or no effect on host angiogenesis. Additional evidence for
271 SOX18 regulation of the MVP was obtained from *RaOp* SOX18 expressing HUVEC. The *RaOp* dominant
272 negative SOX18, which is thought to "poison" normal SOX18 function (33), downregulated HMGCS1 and
273 HMGCR. SOX18 and SREBP2 were found to colocalize in endothelial nuclei in proliferating phase IH and
274 two cases of regrowing IH but not in involuting phase IH or normal skin indicating nuclear SOX18 and
275 SREBP2 may be restricted to nascent vessels in IH. Regrowing IH defies the classic IH life cycle, and little
276 is known about how or why these IH regrow; most often, regrowing IH involves oral mucosa, such as the
277 lip. Typically, propranolol therapy is restarted to prevent sequelae. In our two IH patients, regrowth
278 occurred at 6 and 9 years of age. The nuclear co-localized SOX18 and SREBP2 in proliferating phase IH
279 and regrowing IH suggests that $SOX18^{+}$/$SREBP2^{+}$ endothelial nuclei may serve as a biomarker for the
280 vasculogenic capacity of the tumor. This may give important biomolecular clues for patients to predict
281 treatment response to statins and may thereby provide a novel theranostic approach.
282
283 SOX18 is a firmly established transcriptional regulator of vascular and lymphatic development, and
284 tumor angiogenesis (11-14, 25, 34). The small molecule inhibitor of SOX18, Sm4, suppresses vascular

285 development in zebrafish and both tumor angio- and lymph-angiogenesis in a breast cancer model (25,
286 26). Notably, while glycolysis and fatty acid oxidation have been well established in physiological and
287 pathological endothelial cell metabolism (35, 36), the MVP has not been implicated as a crucial
288 regulatory pathway. In line with R(+) propranolol downregulation of SQLE (Figure 1C, Supplemental
289 Table 1), the gene encoding squalene epoxidase, a key enzyme in cholesterol biosynthesis, single cell
290 RNA sequencing of endothelial cells in pathological angiogenesis identified SQLE as a metabolic
291 angiogenic target (37). Our discovery of a functional link between SOX18 and the MVP brings to light an
292 entirely novel concept in endothelial differentiation and vasculogenesis. By interfering with SOX18
293 transcriptional activity and downstream regulation of the MVP, R+ propranolol acts as an EC phenotype-
294 specific "statin".
295
296 The MVP is central to cholesterol biosynthesis and isoprenoid biosynthesis, the later needed for
297 prenylation. The MVP bifurcates at farnesyl pyrophosphate (FPP) to produce squalene, an intermediate
298 in cholesterol biosynthesis, or geranylgeranyl pyrophosphate (GGPP). FPP and GGPP are directly
299 involved in prenylation of various small GTPases, and other protein substrates including RAS family
300 members (38). Importantly, RAS signaling has been implicated in IH (39). The R(+) propranolol mediated
301 reduction in MVP genes and cholesterol biosynthesis may affect membrane fluidity and ruffling or
302 activation of important signaling pathways by prenylation. This warrants further investigation.
303
304 Pleiotropic benefits of statins, beyond their lowering effect on plasma LDL-cholesterol levels, are well
305 documented and thus inferred to provide cardiovascular disease protection. These include inhibiting
306 inflammatory response, increasing the bioavailability of nitric oxide, promoting re-reendothelialization,
307 and reducing oxidative stress (19, 20, 40). The underlying mechanisms, however, remain elusive. A
308 recent study suggests epigenetic effects: simvastatin significantly improved human induced pluripotent
309 stem cell-derived endothelial cell function by reducing chromatin accessibility under physiological and
310 pathological conditions (24). Moreover, statins block mammalian target of rapamycin (mTOR) and
311 thereby inhibit AKT signaling (41), which is central to balancing vascular growth with endothelial
312 quiescence. It was further shown that mTOR complex 1 reduces ER cholesterol levels which in turn
313 activates SREBP2 and the MVP (42). Of note, PI3K-AKT-mTOR signaling is crucial in the pathogenesis of
314 slow-flow vascular malformations (43, 44). Hence, statins may hold promise to be efficient in these
315 vascular anomalies as well and may be relevant for future directions.

316 Statins are widely used drugs. The resulting reduction in cholesterol synthesis consequently increases
317 LDL-receptor expression, which in turn, clears low-density lipoprotein cholesterol from the circulation.
318 Although statins are generally considered a safe and well tolerated drug class, they are associated with
319 an increased risk of muscle pain, diabetes mellitus and hepatic transaminase elevations (45). We
320 addressed potential side effects by measuring glucose levels and body weight in the statin treated
321 xenograft mice. We did not observe a change in glucose levels or weight with simvastatin and
322 atorvastatin over the treatment course of 7 days. This is a relatively short treatment duration to detect
323 adverse effects and moreover, side effects in rodents differ from those in humans. Bearing in mind drug
324 safety as the highest priority when considering translating statins to infants, we performed a dose
325 response experiment with simvastatin. The lowest dose that showed significant reduction in IH vessels
326 in the xenograft model was 1 mg/kg/d (Figure 5). This translates to a human equivalent dose of 0.081
327 mg/kg/d (46) (Supplemental Figure 5, Table S5.2), which is 6.25 times below the recommended dose of
328 0.5 mg/kg/d systemic simvastatin for infants with other indications. Further, topical rather than systemic
329 statins might be used for superficial or less complex IH with increased safety as shown for other
330 applications discussed below.
331
332 Systemic statins have been used safely in infants with Smith-Lemli-Opitz syndrome (SLOS). In a
333 randomized, placebo-controlled clinical trial the recommended dose was 0.5 to a maximum of 1
334 mg/kg/d. SLOS is an autosomal-recessive multiple malformation/cognitive impairment syndrome and
335 characterized by the accumulation of 7-dehydrocholesterol, a precursor of cholesterol (31, 47-49).
336 Topical statins have also been used for dermatological conditions such as congenital hemidysplasia with
337 ichthyosiform erythroderma and limb defects (CHILD) syndrome - an X-linked, dominant condition with
338 most surviving patients being female (50). In addition, statins have been used to treat alopecia areata
339 (51, 52). Based on the successful use of statins in children with these disorders, we suggest a safe
340 repurposing of topical and systemic simvastatin to treat infants with IH.
341
342 It is exciting to speculate that the novel link between SOX18 and the MVP may have important
343 implications for various pathophysiological conditions of the endothelium, including developmental
344 defects in vascular anomalies and other disease scenarios with disturbed vasculogenesis and
345 angiogenesis. In contrast to vascular malformations for which genetic drivers have been identified in
346 recent years, the genetic basis of IH is unknown. The advanced understanding of genetics has facilitated
347 targeted therapies for vascular malformations translating pre-existing oncology drugs that interfere with

348 signaling pathways involved (53, 54). Conversely, critical molecular players in IH have been uncovered by
349 studying mechanisms of action of serendipitously discovered drugs (8, 9, 55, 56). This has led to our
350 discovery that demonstrates a mechanistic link between beta-blockers and statins via the endothelial
351 cell specific transcription factor SOX18.
352
353 We propose the SOX18-MVP-axis may connect broadly to clinical studies that link beta-blocker and
354 statin use to improved outcomes in cancer patients. We speculate this is due to suppression of the
355 SOX18-MVP-axis in tumor endothelial cells and in turn, tumor angiogenesis. Propranolol is currently
356 being studied as single administration adjuvant therapy or in combination with standard therapies in
357 several clinical trials (57). Statin use was first found associated with improved outcomes in colorectal
358 cancer patients in 2005 (58) and subsequent studies confirmed this observation and extend to post-
359 diagnosis statin use (59-64).
360
361 In summary, our findings uncover a novel SOX18-MVP axis as a central molecular driver for HemSC
362 vasculogenesis. In a xenograft model we show that simvastatin or atorvastatin inhibit IH vessel
363 formation. This suggests statins could be repurposed to treat this common vascular tumor of infancy,
364 topically or systemically. Moreover, we demonstrate suppression of the transcription of MVP genes via
365 R+ propranolol disruption of SOX18. This provides a mechanistic link between two of the most widely
366 used drugs in cardiovascular disease – beta-blockers and statins. We propose that the SOX18-MVP axis
367 may explain the pleiotropic effects of beta-blockers and statins in a wide range of clinical scenarios that
368 involve pathological vasculogenesis and angiogenesis.

369 **METHODS:**

370 *IH cell isolation and culture:* The clinical diagnosis of IH was confirmed in the Department of Pathology of
371 Boston Children's Hospital. Single-cell suspensions prepared from proliferating IH specimens were de-
372 identified and designated as specified in Table 1. HemSC or HemEC were selected using anti-CD133– and
373 anti-CD31–coated magnetic beads (Miltenyi Biotec), respectively, and expanded. Testing for
374 mycoplasma contamination by qPCR was performed when cells were thawed and every 4–6 weeks
375 thereafter. Cells were cultured on fibronectin-coated (0.1 µg /cm^2; MilliporeSigma) plates with a density
376 of 20,000 cells/cm^2 with Endothelial Growth Medium-2 (EGM-2; Lonza), which consists of Endothelial
377 Growth Basal Medium-2 (EBM-2; Lonza), SingleQuots supplements (all except hydrocortisone and
378 gentamicin-1000; Lonza), 10% heat-inactivated FBS (Cytiva), and 1× GPS (292 mg/mL glutamine, 100
379 U/mL penicillin, 100 mg/mL streptomycin, Mediatech). Hereafter, this full growth media is referred to as
380 EGM-2. Cells were cultured at 37°C in a humidified incubator with 5% CO_2 and fed every other day.
381

382 *Hemangioma endothelial differentiation assay:* To induce endothelial differentiation, HemSC (samples
383 denoted as HemSC 125, 149, 150, 165, 167, 171) were seeded on fibronectin-coated plates (0.01 µg
384 fibronectin/cm^2) at a density of 20,000 cells/cm^2 in EGM-2. After 18 - 24 hours, cells were starved for 16
385 hours in 2% BSA/serum-free EBM-2. Cells were washed with EBM-2 once. The medium was replaced by
386 differentiation media that consisted of serum-free EBM-2 containing 1× insulin transferrin-selenium,
387 1:100 linoleic acid–albumin, 1 µM dexamethasone, and 100 µM ascorbic acid-2-phosphate. The medium
388 was replaced with fresh differentiation medium containing 10 ng/mL VEGF-B (R&D Systems) every two
389 days. For addition of inhibitors, a preincubation ± respective inhibitors (R(+) propranolol, simvastatin, or
390 atorvastatin) for 30 minutes was conducted followed by continuous treatment. Stock solutions of 10
391 mM R(+) propranolol hydrochloride (MilliporeSigma), 105 mM simvastatin, and 10mM atorvastatin
392 (both Selleckchem) were prepared in DMSO (MilliporeSigma). 20 µM R(+) propranolol was added for
393 two hours and cells harvested (n=6) for RNA sequencing (Figure 1A,B,C). Continuous (4 consecutive
394 days) as well as short term treatment (2 hours) with 20 µM R(+) propranolol was applied to validate the
395 RNA sequencing data of HemSC undergoing endothelial differentiation by qPCR (n=3) (Figure 1D,E).
396 Continuous treatment with 1 µM simvastatin, 0.1 µM atorvastatin as well as 20 µM R(+) propranolol as a
397 positive control was applied to differentiating HemSC (n=3) to test for an effect of statins in vitro (Figure
398 5A). Respective vehicle controls of each drug were used. Vehicle without VEGF-B served as a negative
399 control and with VEGF-B as a positive control for differentiation. A potential toxic effect of simvastatin

400 and atorvastatin on viability of HemSC (n=3) ± simvastatin, atorvastatin, or vehicle incubated for 24
401 hours was assessed by cell counting (Supplemental Figure 5.1).

402 *Cholesterol measurements in HUVEC:* HUVEC were grown in EBM-2 media (Lonza, CC-3156) and
403 supplemented with EGM-2 bullet kit (Lonza, CC-3162). HUVEC were seeded on 0.5% gelatin-coated 6-
404 well plates at a density of 1.5 x10^5 cells/well overnight. The day after seeding cells were treated with
405 MBCD (Sigma C4555) at a concentration of 2.5 mM to deplete cells of endogenous cholesterol. MBCD
406 was withdrawn after 4 hours and cells were washed with PBS. After this, cells were treated with either
407 PBS, 20 µM R(+) propranolol (Sigma-Aldrich, Cat P0689), DMSO, or 40 µM of Sm4 (Sigma-Aldrich,
408 SML1999) for 18 hours. Cells were then washed with PBS, trypsinized, washed with PBS, and
409 centrifuged (Figure 2B,C). Lipids were extracted from the cell pellets through one-phase extraction with
410 202 uL of BuOH:MeOH (1:1) (Sigma 71-36-3 and 67-56-1) that contains 10 umol of cholesterol-d7
411 (Cayman Chemical 83199-47-7) as the internal standard (65). The cholesterol analysis was performed on
412 a TSQ Altis triple quadrupole mass spectrometer, operated in positive ion mode, coupled to a Vanquish
413 UHPLC system (Thermo Fisher, Waltham, USA) using the transition from precursor mass of *m/z* 369.3516
414 (MS1) to *m/z* 161.1 (MS3) for cholesterol and 376.4 to 161.1 for cholesterol-d7 (65). The solvent pair
415 included solvent A (100% H2O, 0.1% FA and 2 mM NH_4COO^-) and solvent B (100% MeOH, 0.1% FA and 2
416 mM NH_4COO^-) with a flow rate at 0.3 mL/min (80% B at the start). Cholesterol and its deuterated
417 standard were separated on an Eclipse Plus C8 column (Agilent), and peaks were integrated with
418 TraceFinder 5.1 (Thermo Fisher, Waltham, USA) using the daughter ion at *m/z* 161.1 (Figure 2B,C) (66).

419 *RaOp expression in HUVECs:* The day after HUVEC seeding, transfection was performed using X-
420 tremeGene HP Transfection Reagent kit (Roche) to introduce 500ng of Halo-RaOp DNA using EBM-2
421 culture media without antibiotic. Cells were incubated at 37°C with 5% CO_2 overnight. The next day, cells
422 were incubated with 5nM of JF646-Halo-ligand for 15min, washed with PBS and trypsinized; as a result,
423 HUVEC expressing $SOX18^{RaOp}$ were fluorescently tagged. Cells were spun down, washed with PBS and
424 permeabilized with 0.2% Triton X-100 for 10min, following blocking with 5% BSA/PBS for 1 hour. Cells
425 were labelled with 1:300 dilution of anti-human HMGCR (ThermoFisher, PA537367) or HMGCS1
426 (ThermoFisher, PA513604) for 1 hour at room temperature in the dark. Cells were washed with PBS and
427 stained with 1:500 dilution of anti-rabbit IgG conjugated with Alexa Fluor 488 (Invitrogen A11008) for 30
428 min and washed with PBS. Cells were then imaged on a Fortessa X-20 (BD Bioscience). Data analysis was
429 performed using FlowJo software (Figure 2D,E).

430 *shRNA knockdown of SOX18:* HemEC (n=3) were transduced with SOX18 shRNA lentivirus
431 (TRCN0000017450, Sigma) or an empty vector control virus (Sigma SHC001V) followed by puromycin (1
432 µg/mL) selection for 5 days. Thereafter, cells were maintained in EGM-2 without puromycin. Knockdown
433 efficiency was confirmed by qPCR and Western Blot (Figure 3C-G, Supplemental Figure 3.1,2).
434
435 *Western Blot:* HemSC were seeded on fibronectin-coated plates (0.1 µg fibronectin/cm^2) at a density of
436 20,000 cells/cm^2 in EGM-2. HemSC were induced to undergo differentiation according to the protocol
437 described above. Cells were treated with 20 µM R(+) propranolol for 2 hours on Day 6 of endothelial
438 differentiation and lysed in a RIPA-based lysis buffer (25 mM Tris HCl pH 7.6, 150 mM NaCl, 1% NP-40,
439 1% sodium deoxycholate, 0.1% SDS) with protease and phosphatase inhibitors (Cell Signaling
440 Technology, 5872S) as well as a calpain I and proteasome V inhibitors (Millipore Sigma, 208719). Cell
441 extracts were electrophoresed by sodium dodecyl sulfate-polyacrylamide gel electrophoresis (SDS-
442 PAGE), transferred to nitrocellulose or to polyvinylidene difluoride (PDVF) and probed with anti-SREBP2
443 clone 22D5 (Millipore Sigma, MAB1988) followed by anti-GAPDH (Cell Signaling Technology, 5174).
444 For protein quantification of shSOX18 knockdown efficiency in $HemEC^{shSOX18}$ (samples denoted as HemEC
445 ^{shSOX18} 133, 150 and 171), cells were seeded on fibronectin-coated plates (0.1 µg fibronectin/cm^2) at a
446 density of 20,000 cells/cm^2 in EGM-2 media, lysed and processed as described above following staining
447 with SOX18 D-8 (Santa Cruz Biotechnology, sc-166025) and GAPDH (Cell Signaling Technology, 5174)
448 antibodies. All signals were detected by enhanced chemiluminescence. The densitometric analysis was
449 conducted using Fiji ImageJ software.
450
451 *In vivo murine model for human blood vessel formation:* In vivo, HemSC undergo vasculogenesis and
452 form anastomoses with ingrowing host vessels. Experiments were carried out with 3×10^6 HemSC per
453 implant. HemSC (n=4, samples 125, 147, 149, 150) were grown in EGM-2 media until 90% confluency. A
454 stock solution of simvastatin (105 mM; MilliporeSigma) or atorvastatin (10 mM; MilliporeSigma) was
455 prepared in DMSO. The stock solution was diluted with PBS to the indicated treatment concentrations.
456 Twenty-four hours before harvesting, 5 µM treatment with simvastatin or 0.5 µM treatment with
457 atorvastatin or the equivalent DMSO concentration (0.005%) as a control was added to the media. Cells
458 were counted after the 24-hour pretreatment and suspended in 200 µL Matrigel (Corning) preadjusted
459 with 1 µg/mL basic FGF (bFGF) (ProSpec), 1 µg/mL erythropoietin (EPO) (ProSpec), and 2.5 µM
460 (simvastatin) or 0.25 µM (atorvastatin) drug or PBS with max 0.005% DMSO on ice. The Matrigel/cell
461 suspensions were injected subcutaneously into the flanks of 6-week-old male athymic nu/nu mice

462 (envigo), placing 2 implants per mouse (n = 3-5 mice/group; Figure 5B). The mice were treated with 0.1 -
463 50 mg/kg/d simvastatin, 1 - 15 mg/kd/d atorvastatin or the equivalent DMSO concentration (maximal
464 11.4 %) as a control (200 µL/mouse, i.p.) twice a day. Blood glucose levels of the mice were measured
465 daily before the morning i.p. injection. Glucose concentrations were measured in tail vein blood using
466 the OneTouch UltraSmart Blood Glucose Monitoring System (LifeScan). Body weight was measured
467 before the injections (day 0), on day 4 and before removal of the implants (day 8). After 8 days, the mice
468 were euthanized and the implants were removed, fixed in formalin, embedded in paraffin, and analyzed
469 by H&E staining and immunofluorescent staining (IF). Blood vessels (indicated by luminal structures
470 containing one or more red blood cells) and $CD31^+$ stained human vessels were counted in 5
471 fields/section, 2 sections/implant. Each field was 425.1 µm × 425.1 µm = 0.18071 mm2, and sections
472 were from the middle of the implant. Vessel density is expressed as vessels/mm^2.

473 *Histology and IF analysis:* FFPE tissue sections (5 µm) of the Matrigel implants were deparaffinized and
474 either directly stained with H&E or immersed in an antigen retrieval solution (citrate-EDTA buffer
475 containing 10 mM citric acid, 2 mM EDTA, and 0.05% Tween-20, pH 6.2) for 20 minutes at 95°C–99°C.
476 Sections were subsequently blocked for 30 minutes in TNB Blocking Buffer (PerkinElmer) followed by
477 incubation with an anti-human CD31 monoclonal antibody (1:30, mouse anti-human; Dako, Glostrup,
478 0823) to stain for human endothelium. Next, sections were incubated with Alexa Fluor 647 chicken anti-
479 mouse IgG (1:200, Invitrogen, Thermo Fisher Scientific) as a secondary antibody (Figure 5C,D).
480 An anti-mouse-specific CD31 monoclonal antibody (1:100, R&D Systems,) was used to quantify mouse
481 vessels in the Matrigel implants. Alexa Fluor 647 chicken anti-goat IgG was applied as a secondary
482 antibody (Supplemental Figure 5.4). Tissue specificity of the anti-human and anti-mouse antibodies was
483 confirmed by negative staining in mouse lung and human skin tissue, respectively (Supplemental Figure
484 5.6).

485 FFPE tissue sections (5 µm) from patients with IH were deparaffinized, immersed in an antigen retrieval
486 solution, and blocked for 30 minutes in 10% donkey serum followed by incubation with mouse anti-
487 human SOX18 (1:50; Santa Cruz Biotechnology), rabbit anti-human SREBP2 and UEA1 fluorescently
488 labeled with Alexa Fluor 649 (1:50; Vector Laboratories). Next, the sections were incubated with Alexa
489 Fluor 488 donkey anti-mouse IgG and Alexa Fluor 546 donkey anti-rabbit IgG (both 1:200; Invitrogen,
490 Thermo Fisher Scientific) as secondary antibodies. All slides were mounted using DAPI (Molecular
491 Probes, R37606) to visualize nuclei. IF Images were acquired by a LSM 880 confocal microscope (Zeiss).

492 Images were analyzed through a 20x or 63x objective lens. All images were analyzed using Fiji ImageJ
493 software (Figure 4).

494 *Cell staining:* HemEC171^{naïve} and HemEC171^{shSOX18} were seeded on fibronectin-coated plates at a density
495 of 20,000 cells/cm^2 in EGM-2 media for 30 hours on 2 cm^2 slides, fixed in 4% PFA and blocked in 5%
496 BSA/0.3% Triton x-100 for 1 hour. The mouse anti-human SOX18 primary antibody used for
497 immunostaining (E-11) was validated in HemEC^{naïve} and HemEC^{shSOX18} (1:100, Santa Cruz, sc-376166),
498 Cells were co-stained with a rabbit anti-human VE-Cadherin (1:100, R&D Systems). Secondary antibodies
499 included Alexa Fluor 488 donkey anti-mouse IgG and Alexa Fluor 546 donkey anti-rabbit IgG (both 1:200;
500 Invitrogen, Thermo Fisher Scientific). Slides were mounted using DAPI (Molecular Probes, R37606) to
501 visualize nuclei (Supplemental Figure 4.5,6). Immunostaining of IH sections with respective isotype
502 matched control IgG and secondary antibodies are shown in (Supplemental Figure 4.7,8).

503 *RNA isolation and qPCR:* Total cellular RNA was extracted from cells with a RNeasy Micro Extraction Kit
504 (QIAGEN). Reverse transcriptase reactions were performed using an iScript cDNA Synthesis Kit (Bio-Rad).
505 qPCR was performed using SYBR FAST ABI Prism 2× qPCR Master Mix (Kapa BioSystems). Amplification
506 was carried out in a QuantStudio 6 Flex Real-Time PCR System (Thermo Fisher Scientific). A relative
507 standard curve for each gene amplification was generated to determine the amplification efficiency,
508 with greater than 90% considered acceptable. Fold increases in gene expression were calculated
509 according to the ΔΔCt method, with each amplification reaction performed in duplicate or triplicate (67).
510 Gene expression was normalized to the PBS treatment. ATP5B was used as housekeeping gene
511 expression reference.

512 *Bioinformatic analysis:*
513 *Bulk RNA-seq:* We used trimmomatic v0.39 (68) to trim the low-quality next generation sequencing
514 (NGS) reads (-threads 20 ILLUMINACLIP:TruSeq3-PE.fa:2:30:10 LEADING:3 TRAILING:3
515 SLIDINGWINDOW:4:15 MINLEN:36). Subsequently, only the high-quality trimmed reads were aligned to
516 the human reference genome (hg38) using STAR v2.7.2b . The reads counts were calculated by
517 featureCounts software (69). Differentially expressed genes (DEGs) were identified by using the DESeq2
518 R package (adjusted p-value < 0.05). KEGG pathways and gene ontology (GO) enrichment tests were
519 performed by the clusterProfiler R package. A pathway or GO term was treated as significantly enriched
520 if an adjusted p-values (with Benjamini-Hochberg correction) was smaller than 0.05. The bar plots
521 illustrating significant pathway or GO terms were created using the enrichplot R package.

522 *ChIP-seq:* The data is displayed on the UCSC genome browser. The layered epigenetic marks dataset is
523 supplied from Encode. ChIP-seq binding location dataset can be found at
524 https://www.ebi.ac.uk/biostudies/arrayexpress/studies/E-MTAB-4481.

525 *Statistics:* Data were analyzed and plotted using GraphPad Prism 10.1.0 (GraphPad Software). Results
526 are displayed as the mean ± SD. For experiments in which cells were treated with alternative drugs, the
527 differences were assessed by one-way ANOVA. Tukey's post hoc test was used for multiple comparisons
528 of different treatment modalities and Šidák's, Tukey's or Dunnett's test for multiple comparisons to
529 compare every treatment mean with that of the vehicle control. A two-tailed, unpaired t-test with was
530 applied for comparisons between treatment and control groups given equal variance.
531

532 *Study approval:* Animal protocols complied with NIH Animal Research Advisory Committee guidelines
533 and were approved by the Boston Children's Hospital Animal Care and Use Committee (protocol number
534 00001741). IH specimens were obtained under a protocol approved by the Committee on Clinical
535 Investigation at Boston Children's Hospital (IRB protocol number 04-12-175R; AH, HK, JBM, JB) as well as
536 at Stanford University (IRB protocol number 35473; RL, JT). Hemangioma specimens were collected
537 upon written informed consent of the patient's guardian, deidentified, and used for cell isolation under
538 a Boston Children's Hospital IRB approved protocol (04-12-175R) and in accordance with Declaration of
539 Helsinki principles.

540

541 **Acknowledgements**

542 We thank the Vascular Anomalies Center and Department of Pathology at Boston Children's Hospital for
543 clinical care and for sharing patient specimens.
544 We thank Trisha Lopez for patient chart reviews, Dr. Sandra Schrenk for her intellectual input and
545 technical advice, Dr. Andrew Stone for imaging advice and Kristin Johnson of the Vascular Biology
546 Program graphics core for figure design. Research reported in this manuscript was funded by NIH grant
547 5R01HL096384-012 (to JB). MF, MG are supported by the National Health and Medical Research Council,
548 GNT1164000. AH was supported by the Deutsche Forschungsgemeinschaft (DFG, German Research
549 Foundation, grant 458322953), and is supported by the Vascular Anomalies Center at Boston Children's
550 Hospital. JWHT received funding from the Nanyang Technological University CN Yang Scholars Program,
551 AH and MV are members of the Vascular Anomalies Working Group (VASCA) of the European Reference
552 Network for Rare Multisystemic Vascular Diseases (VASCERN) - Project ID: 769036.

The funders had no role in the study design, data collection and interpretation, or decision to submit this work for publication.

Author contributions

AH, MG, MF and JB designed the study. AH, MG, JWS, LB, LC, AJ, MS, LS, MF and JB designed the methodology. AH, MG, JWS, LB, JWHT and LC performed functional investigations. AH, MG, JWS, LB, JWHT, LC, AJ, MS, and LS carried out formal analysis. AH and JB wrote the original draft. All authors performed reviewing and editing. All authors read and agreed to the final version of the manuscript. AH performed patient data curation. RL, HK, JCT and JBM provided patient specimens and clinical expertise. LS, JQ, JCT, MV, MF and JB provided supervision. MF and JB conceived the study. AH, JWHT, MV, MF and JB acquired funding.

Competing interests

MF is involved with the startup biotech company GBM Pty Ltd., which develops SOX18 small-molecule inhibitors. The other authors declare no competing interests.

Intellectual Property

Holm and Bischoff are co-inventors on a filed patent application PCT/US23/83306 “Methods and Compositions for the Treatment of Vascular Anomalies.” Bischoff is co-inventor on US Patent # 9,737,514.

573 **REFERENCES:**

574 1. Leaute-Labreze C, Harper JI, and Hoeger PH. Infantile haemangioma. *Lancet.*
575 2017;390(10089):85-94.
576 2. Leaute-Labreze C, Hoeger P, Mazereeuw-Hautier J, Guibaud L, Baselga E, Posiunas G, et
577 al. A randomized, controlled trial of oral propranolol in infantile hemangioma. *N Engl J*
578 *Med.* 2015;372(8):735-46.
579 3. Leaute-Labreze C, Boccara O, Degrugillier-Chopinet C, Mazereeuw-Hautier J, Prey S,
580 Lebbe G, et al. Safety of Oral Propranolol for the Treatment of Infantile Hemangioma: A
581 Systematic Review. *Pediatrics.* 2016;138(4).
582 4. Pope E. Commentary:Beta-blockers and sleep problems. *Pediatr Dermatol.*
583 2021;38(2):378-9.
584 5. Hermans MM, Rietman AB, Schappin R, de Laat PCJ, Mendels EJ, Breur J, et al. Long-
585 term neurocognitive functioning of children treated with propranolol or atenolol for
586 infantile hemangioma. *Eur J Pediatr.* 2023;182(2):757-67.
587 6. Mehvar R, and Brocks DR. Stereospecific pharmacokinetics and pharmacodynamics of
588 beta-adrenergic blockers in humans. *J Pharm Pharm Sci.* 2001;4(2):185-200.
589 7. Khan ZA, Boscolo E, Picard A, Psutka S, Melero-Martin JM, Bartch TC, et al.
590 Multipotential stem cells recapitulate human infantile hemangioma in immunodeficient
591 mice. *Journal of Clinical Investigation.* 2008;118(7):2592-9.
592 8. Overman J, Fontaine F, Wylie-Sears J, Moustaqil M, Huang L, Meurer M, et al. R-
593 propranolol is a small molecule inhibitor of the SOX18 transcription factor in a rare
594 vascular syndrome and hemangioma. *Elife.* 2019;8.
595 9. Seebauer CT, Graus MS, Huang L, McCann A, Wylie-Sears J, Fontaine F, et al. Non-beta
596 blocker enantiomers of propranolol and atenolol inhibit vasculogenesis in infantile
597 hemangioma. *J Clin Invest.* 2022;132(3).
598 10. Irrthum A, Devriendt K, Chitayat D, Matthijs G, Glade C, Steijlen PM, et al. Mutations in
599 the transcription factor gene SOX18 underlie recessive and dominant forms of
600 hypotrichosis-lymphedema-telangiectasia. *Am J Hum Genet.* 2003;72(6):1470-8.
601 11. Patel J, Seppanen EJ, Rodero MP, Wong HY, Donovan P, Neufeld Z, et al. Functional
602 Definition of Progenitors Versus Mature Endothelial Cells Reveals Key SoxF-Dependent
603 Differentiation Process. *Circulation.* 2017;135(8):786-805.
604 12. Herpers R, van de Kamp E, Duckers HJ, and Schulte-Merker S. Redundant roles for sox7
605 and sox18 in arteriovenous specification in zebrafish. *Circ Res.* 2008;102(1):12-5.
606 13. Francois M, Caprini A, Hosking B, Orsenigo F, Wilhelm D, Browne C, et al. Sox18 induces
607 development of the lymphatic vasculature in mice. *Nature.* 2008;456(7222):643-7.
608 14. Young N, Hahn CN, Poh A, Dong C, Wilhelm D, Olsson J, et al. Effect of disrupted SOX18
609 transcription factor function on tumor growth, vascularization, and endothelial
610 development. *J Natl Cancer Inst.* 2006;98(15):1060-7.
611 15. Zhang C, Jin DD, Wang XY, Lou L, and Yang J. Key Enzymes for the Mevalonate Pathway
612 in the Cardiovascular System. *J Cardiovasc Pharmacol.* 2021;77(2):142-52.
613 16. Horton JD, Goldstein JL, and Brown MS. SREBPs: activators of the complete program of
614 cholesterol and fatty acid synthesis in the liver. *J Clin Invest.* 2002;109(9):1125-31.

615 17. Yamauchi Y, Iwamoto N, Rogers MA, Abe-Dohmae S, Fujimoto T, Chang CC, et al.
616 Deficiency in the Lipid Exporter ABCA1 Impairs Retrograde Sterol Movement and
617 Disrupts Sterol Sensing at the Endoplasmic Reticulum. *J Biol Chem.* 2015;290(39):23464-
618 77.
619 18. Chou R, Dana T, Blazina I, Daeges M, and Jeanne TL. Statins for Prevention of
620 Cardiovascular Disease in Adults: Evidence Report and Systematic Review for the US
621 Preventive Services Task Force. *JAMA.* 2016;316(19):2008-24.
622 19. Laufs U, La Fata V, Plutzky J, and Liao JK. Upregulation of endothelial nitric oxide
623 synthase by HMG CoA reductase inhibitors. *Circulation.* 1998;97(12):1129-35.
624 20. Sen-Banerjee S, Mir S, Lin Z, Hamik A, Atkins GB, Das H, et al. Kruppel-like factor 2 as a
625 novel mediator of statin effects in endothelial cells. *Circulation.* 2005;112(5):720-6.
626 21. Greenwood J, and Mason JC. Statins and the vascular endothelial inflammatory
627 response. *Trends Immunol.* 2007;28(2):88-98.
628 22. Karlic H, Thaler R, Gerner C, Grunt T, Proestling K, Haider F, et al. Inhibition of the
629 mevalonate pathway affects epigenetic regulation in cancer cells. *Cancer Genet.*
630 2015;208(5):241-52.
631 23. Tikoo K, Patel G, Kumar S, Karpe PA, Sanghavi M, Malek V, et al. Tissue specific up
632 regulation of ACE2 in rabbit model of atherosclerosis by atorvastatin: role of epigenetic
633 histone modifications. *Biochem Pharmacol.* 2015;93(3):343-51.
634 24. Liu C, Shen M, Tan WLW, Chen IY, Liu Y, Yu X, et al. Statins improve endothelial function
635 via suppression of epigenetic-driven EndMT. *Nat Cardiovasc Res.* 2023;2(5):467-85.
636 25. Overman J, Fontaine F, Moustaqil M, Mittal D, Sierecki E, Sacilotto N, et al.
637 Pharmacological targeting of the transcription factor SOX18 delays breast cancer in
638 mice. *Elife.* 2017;6.
639 26. Fontaine F, Overman J, Moustaqil M, Mamidyala S, Salim A, Narasimhan K, et al. Small-
640 Molecule Inhibitors of the SOX18 Transcription Factor. *Cell Chem Biol.* 2017;24(3):346-
641 59.
642 27. Pennisi D, Gardner J, Chambers D, Hosking B, Peters J, Muscat G, et al. Mutations in
643 Sox18 underlie cardiovascular and hair follicle defects in ragged mice. *Nat Genet.*
644 2000;24(4):434-7.
645 28. Radhakrishnan A, Goldstein JL, McDonald JG, and Brown MS. Switch-like control of
646 SREBP-2 transport triggered by small changes in ER cholesterol: a delicate balance. *Cell*
647 *Metab.* 2008;8(6):512-21.
648 29. Chen L, Ma MY, Sun M, Jiang LY, Zhao XT, Fang XX, et al. Endogenous sterol
649 intermediates of the mevalonate pathway regulate HMGCR degradation and SREBP-2
650 processing. *J Lipid Res.* 2019;60(10):1765-75.
651 30. Downes M, and Koopman P. SOX18 and the transcriptional regulation of blood vessel
652 development. *Trends Cardiovasc Med.* 2001;11(8):318-24.
653 31. Wassif CA, Kratz L, Sparks SE, Wheeler C, Bianconi S, Gropman A, et al. A placebo-
654 controlled trial of simvastatin therapy in Smith-Lemli-Opitz syndrome. *Genet Med.*
655 2017;19(3):297-305.
656 32. Jones P, Kafonek S, Laurora I, and Hunninghake D. Comparative dose efficacy study of
657 atorvastatin versus simvastatin, pravastatin, lovastatin, and fluvastatin in patients with
658 hypercholesterolemia (the CURVES study). *Am J Cardiol.* 1998;81(5):582-7.

659 33. McCann AJ, Lou J, Moustaqil M, Graus MS, Blum A, Fontaine F, et al. A dominant-
660 negative SOX18 mutant disrupts multiple regulatory layers essential to transcription
661 factor activity. *Nucleic Acids Res.* 2021;49(19):10931-55.
662 34. Donovan P, Patel J, Dight J, Wong HY, Sim SL, Murigneux V, et al. Endovascular
663 progenitors infiltrate melanomas and differentiate towards a variety of vascular beds
664 promoting tumor metastasis. *Nat Commun.* 2019;10(1):18.
665 35. Eelen G, de Zeeuw P, Treps L, Harjes U, Wong BW, and Carmeliet P. Endothelial Cell
666 Metabolism. *Physiol Rev.* 2018;98(1):3-58.
667 36. Zeng Q, Mousa M, Nadukkandy AS, Franssens L, Alnaqbi H, Alshamsi FY, et al.
668 Understanding tumour endothelial cell heterogeneity and function from single-cell
669 omics. *Nat Rev Cancer.* 2023;23(8):544-64.
670 37. Rohlenova K, Goveia J, Garcia-Caballero M, Subramanian A, Kalucka J, Treps L, et al.
671 Single-Cell RNA Sequencing Maps Endothelial Metabolic Plasticity in Pathological
672 Angiogenesis. *Cell Metab.* 2020;31(4):862-77 e14.
673 38. Palsuledesai CC, and Distefano MD. Protein prenylation: enzymes, therapeutics, and
674 biotechnology applications. *ACS Chem Biol.* 2015;10(1):51-62.
675 39. Hu W, Liu Z, Salato V, North PE, Bischoff J, Kumar SN, et al. NOGOB receptor-mediated
676 RAS signaling pathway is a target for suppressing proliferating hemangioma. *JCI Insight.*
677 2021;6(3).
678 40. Wolfrum S, Jensen KS, and Liao JK. Endothelium-dependent effects of statins.
679 *Arterioscler Thromb Vasc Biol.* 2003;23(5):729-36.
680 41. Lashgari NA, Roudsari NM, Zadeh SST, Momtaz S, Abbasifard M, Reiner Z, et al. Statins
681 block mammalian target of rapamycin pathway: a possible novel therapeutic strategy
682 for inflammatory, malignant and neurodegenerative diseases. *Inflammopharmacology.*
683 2023;31(1):57-75.
684 42. Eid W, Dauner K, Courtney KC, Gagnon A, Parks RJ, Sorisky A, et al. mTORC1 activates
685 SREBP-2 by suppressing cholesterol trafficking to lysosomes in mammalian cells. *Proc*
686 *Natl Acad Sci U S A.* 2017;114(30):7999-8004.
687 43. Seront E, Van Damme A, Boon LM, and Vikkula M. Rapamycin and treatment of venous
688 malformations. *Curr Opin Hematol.* 2019;26(3):185-92.
689 44. Van Damme A, Seront E, Dekeuleneer V, Boon LM, and Vikkula M. New and Emerging
690 Targeted Therapies for Vascular Malformations. *Am J Clin Dermatol.* 2020;21(5):657-68.
691 45. Cholesterol Treatment Trialists C. Effect of statin therapy on muscle symptoms: an
692 individual participant data meta-analysis of large-scale, randomised, double-blind trials.
693 *Lancet.* 2022;400(10355):832-45.
694 46. Nair AB, and Jacob S. A simple practice guide for dose conversion between animals and
695 human. *J Basic Clin Pharm.* 2016;7(2):27-31.
696 47. Jira PE, Wevers RA, de Jong J, Rubio-Gozalbo E, Janssen-Zijlstra FS, van Heyst AF, et al.
697 Simvastatin. A new therapeutic approach for Smith-Lemli-Opitz syndrome. *J Lipid Res.*
698 2000;41(8):1339-46.
699 48. Chan YM, Merkens LS, Connor WE, Roullet JB, Penfield JA, Jordan JM, et al. Effects of
700 dietary cholesterol and simvastatin on cholesterol synthesis in Smith-Lemli-Opitz
701 syndrome. *Pediatr Res.* 2009;65(6):681-5.

702 49. Svoboda MD, Christie JM, Eroglu Y, Freeman KA, and Steiner RD. Treatment of Smith-
703 Lemli-Opitz syndrome and other sterol disorders. *Am J Med Genet C Semin Med Genet.*
704 2012;160C(4):285-94.
705 50. Christiansen AG, Koppelhus U, and Sommerlund M. Skin Abnormalities in CHILD
706 Syndrome Successfully Treated with Pathogenesis-based Therapy. *Acta Derm Venereol.*
707 2015;95(6):752-3.
708 51. Cervantes J, Jimenez JJ, DelCanto GM, and Tosti A. Treatment of Alopecia Areata with
709 Simvastatin/Ezetimibe. *J Investig Dermatol Symp Proc.* 2018;19(1):S25-S31.
710 52. Shin JM, Jung KE, Yim SH, Rao B, Hong D, Seo YJ, et al. Putative therapeutic mechanisms
711 of simvastatin in the treatment of alopecia areata. *J Am Acad Dermatol.* 2021;84(3):782-
712 4.
713 53. Queisser A, Seront E, Boon LM, and Vikkula M. Genetic Basis and Therapies for Vascular
714 Anomalies. *Circ Res.* 2021;129(1):155-73.
715 54. Dompmartin A, Baselga E, Boon LM, Diociaiuti A, Dvorakova V, El Hachem M, et al. The
716 VASCERN-VASCA Working Group Diagnostic and Management Pathways for Venous
717 Malformations. *J Vasc Anom (Phila).* 2023;4(2):e064.
718 55. Greenberger S, Boscolo E, Adini I, Mulliken JB, and Bischoff J. Corticosteroid suppression
719 of VEGF-A in infantile hemangioma-derived stem cells. *N Engl J Med.*
720 2010;362(11):1005-13.
721 56. Greenberger S, Yuan S, Walsh LA, Boscolo E, Kang KT, Matthews B, et al. Rapamycin
722 suppresses self-renewal and vasculogenic potential of stem cells isolated from infantile
723 hemangioma. *The Journal of investigative dermatology.* 2011;131(12):2467-76.
724 57. Albinana V, Gallardo-Vara E, Casado-Vela J, Recio-Poveda L, Botella LM, and Cuesta AM.
725 Propranolol: A "Pick and Roll" Team Player in Benign Tumors and Cancer Therapies. *J*
726 *Clin Med.* 2022;11(15).
727 58. Poynter JN, Gruber SB, Higgins PD, Almog R, Bonner JD, Rennert HS, et al. Statins and
728 the risk of colorectal cancer. *N Engl J Med.* 2005;352(21):2184-92.
729 59. Nielsen SF, Nordestgaard BG, and Bojesen SE. Statin use and reduced cancer-related
730 mortality. *N Engl J Med.* 2012;367(19):1792-802.
731 60. Mamtani R, Lewis JD, Scott FI, Ahmad T, Goldberg DS, Datta J, et al. Disentangling the
732 Association between Statins, Cholesterol, and Colorectal Cancer: A Nested Case-Control
733 Study. *PLoS Med.* 2016;13(4):e1002007.
734 61. Voorneveld PW, Reimers MS, Bastiaannet E, Jacobs RJ, van Eijk R, Zanders MMJ, et al.
735 Statin Use After Diagnosis of Colon Cancer and Patient Survival. *Gastroenterology.*
736 2017;153(2):470-9 e4.
737 62. Li Y, He X, Ding Y, Chen H, and Sun L. Statin uses and mortality in colorectal cancer
738 patients: An updated systematic review and meta-analysis. *Cancer Med.* 2019;8(6):3305-
739 13.
740 63. Pereira M, Matuszewska K, Glogova A, and Petrik J. Mutant p53, the Mevalonate
741 Pathway and the Tumor Microenvironment Regulate Tumor Response to Statin Therapy.
742 *Cancers (Basel).* 2022;14(14).
743 64. Scott OW, TinTin S, Harborg S, Kuper-Hommel MJJ, Lawrenson R, and Elwood JM. Post-
744 diagnostic statin use and breast cancer-specific mortality: a population-based cohort
745 study. *Breast Cancer Res Treat.* 2023;199(1):195-206.

746 65. Huynh K, Barlow CK, Jayawardana KS, Weir JM, Mellett NA, Cinel M, et al. High-
747 Throughput Plasma Lipidomics: Detailed Mapping of the Associations with
748 Cardiometabolic Risk Factors. *Cell Chemical Biology.* 2019;26(1):71-84.e4.
749 66. Liu XT, Chung LH, Liu D, Chen J, Huang Y, Teo JD, et al. Ablation of sphingosine kinase 2
750 suppresses fatty liver-associated hepatocellular carcinoma via downregulation of
751 ceramide transfer protein. *Oncogenesis.* 2022;11(1).
752 67. Schmittgen TD, and Livak KJ. Analyzing real-time PCR data by the comparative C(T)
753 method. *Nat Protoc.* 2008;3(6):1101-8.
754 68. Bolger AM, Lohse M, and Usadel B. Trimmomatic: a flexible trimmer for Illumina
755 sequence data. *Bioinformatics.* 2014;30(15):2114-20.
756 69. Liao Y, Smyth GK, and Shi W. featureCounts: an efficient general purpose program for
757 assigning sequence reads to genomic features. *Bioinformatics.* 2014;30(7):923-30.

758

Table 1: Overview of patient cells and tissues used throughout the study

Sample ID	Gender	Age at resection	Figure
Proliferating IH (<1 year)			
P-150	M	3m	1, 3, 4, 5
P-147	M	3m	4, 5
P-138	F	3m	4
P-133	M	3m	4, 5
P-171	F	4m	1, 3, 4, 5
P-165	F	4m	1, 3, 5
P-168	F	5m	4
P-125	F	5m	1, 4
P-167	F	7m	1, 4
P-149	F	7m	1, 3, 4, 5
Involuting IH (>1 year)			
I-69	F	1y 1m	4
I-79	F	1y 6m	4
I-71	F	2y 1m	4
I-85	M	2y 2m	4
I-99	M	2y 6m	4
I-84	M	2y 6m	4
I-78	M	2y 6m	4
I-67	M	2y 6m	4
I-81	F	2y 11m	4
I-68	F	2y 11m	4
Rebounding IH			
R-1	F	6y 4m	4
R-2	F	9y 6m	4
Skin Controls			
C-1	F	8m	4
C-2	M	1y	4
C-3	M	3y 7m	4
C-4	M	5y 4m	4

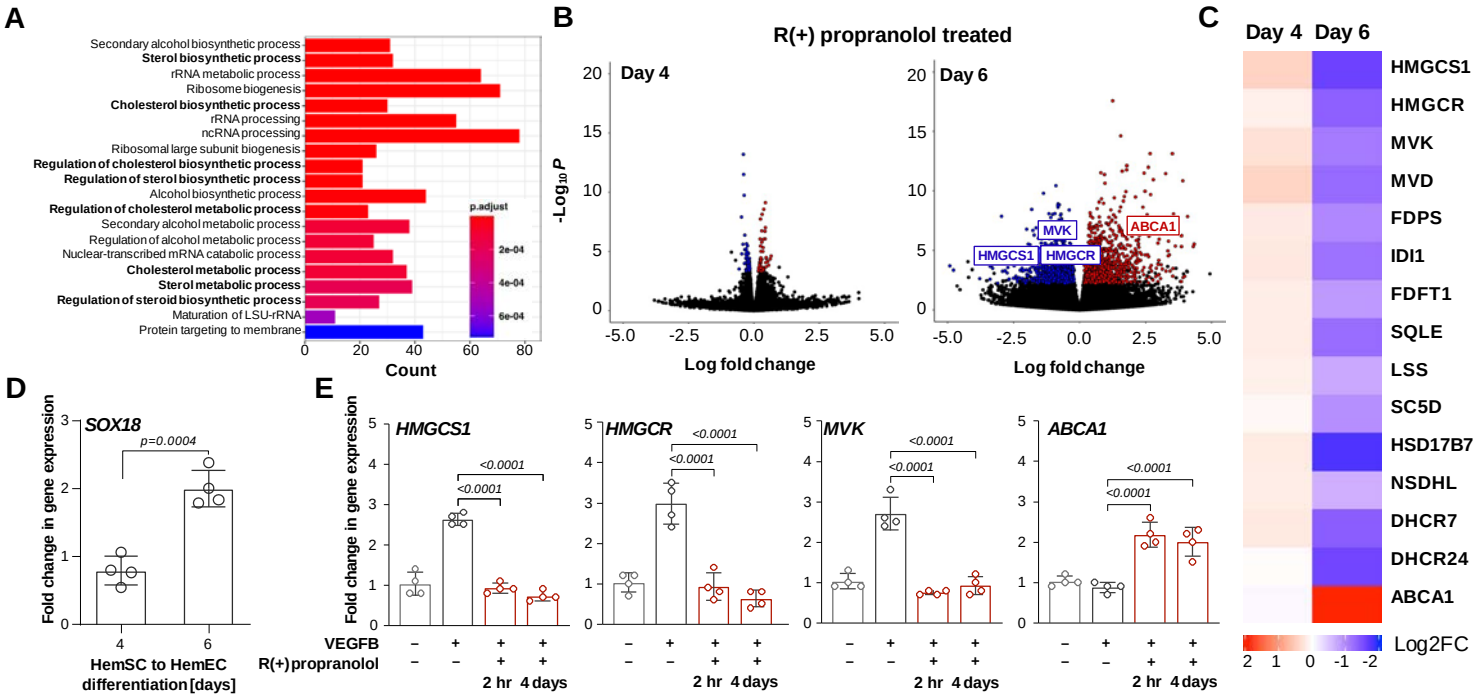

Figure 1. R(+) propranolol reduces MVP transcripts in IH -derived HemSC undergoing endothelial differentiation. (**A**) Gene ontology analysis of the subontology *biological processes* of bulk RNA-seq data set from IH-derived HemSC (n=6). (**B**) Volcano plots show an increase in differentially expressed genes on Day 6 compared to Day 4 of HemSC to endothelial differentiation. (**C**) Heat map with MVP gene transcripts at Day 4 and Day 6 as well as ABCA1 – a negative regulator of the MVP transcription factor SREBP2**.** (**D**) SOX18 measured by qPCR is significantly increased on Day 6 compared to Day 4 (n=3). (**E**) HemSC induced to undergo endothelial differentiation were treated with R+ propranolol for 2 hours on Day 6, or from Day 2-6, i.e., 4-day treatment. qPCR analyses for three MVP genes - *HMGCS1*, *HMGCR*, *MVK,* as well as *ABCA1,* a negative regulator of the MVP transcription factor SREBP2 (n=4). P values were calculated using a 2-tailed, unpaired t-test (**D**) and by a one-way ANOVA multiple comparisons test with Šidák-correction (**E**). Data show the mean ± SD. Data represent sample sizes n=4 (**D**,**E**).

Figure 1

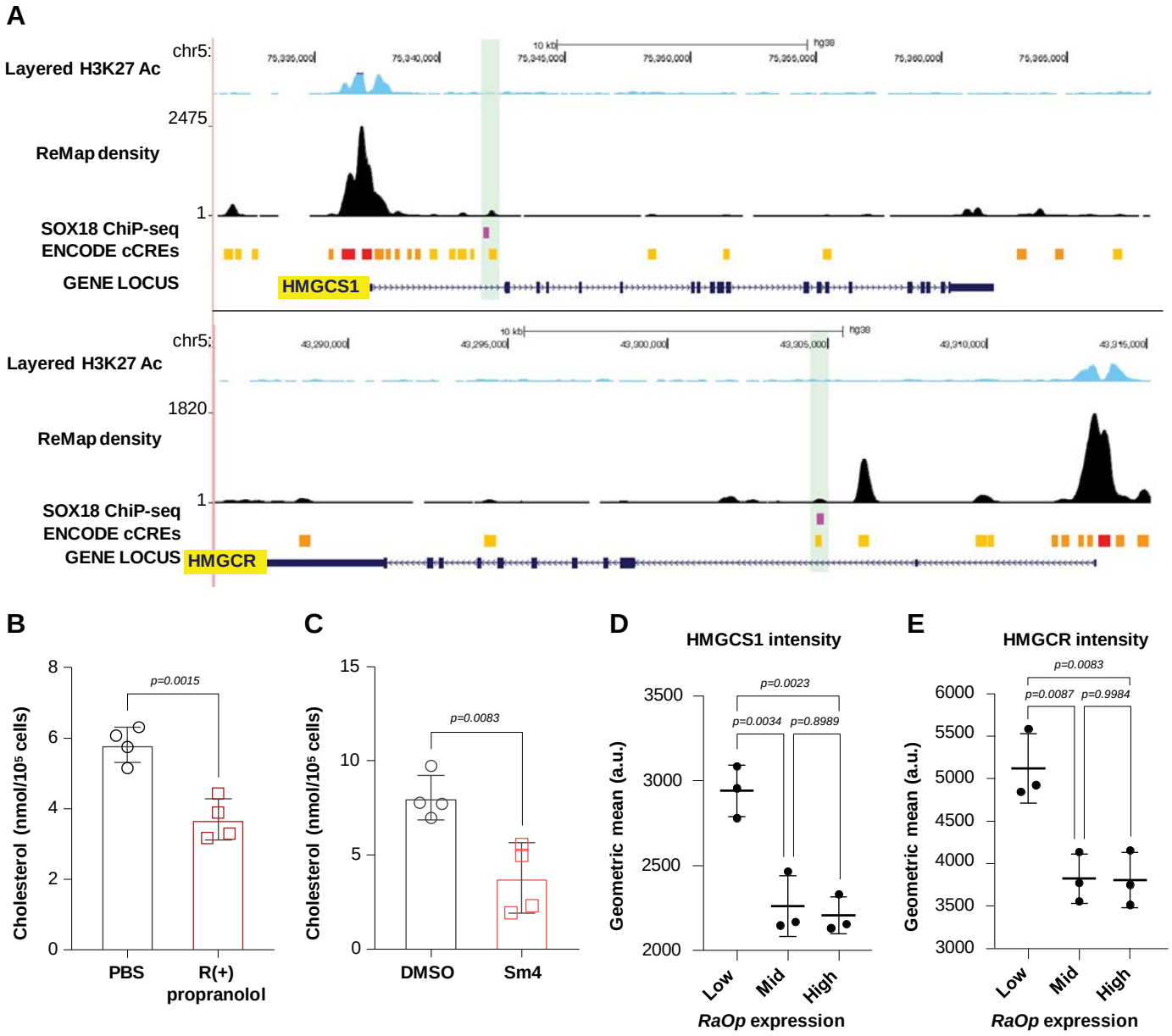

Figure 2. **SOX18 regulates the MVP in endothelial cells.** (**A**) ChIP-Seq dataset in HUVEC demonstrates SOX18 binding sites within the *HMGCS1* and *HMGCR* gene loci which correspond with ENCODE candidate cis-regulatory elements. (**B**,**C**) A functional role for SOX18 in cholesterol biosynthesis was tested by pharmacological disruption of SOX18 activity with R+ propranolol or the SOX18 inhibitor Sm4. HUVECs were cholesterol depleted by incubation with methyl beta-cyclodextrin (MBCD) for 16 hours, followed by treatment ± R(+) propranolol or ± Sm4 for 16 hours each. Endogenous cholesterol levels were measured by mass spectrometry. (**D**,**E**) Overexpression of Ragged Opossum (*RaOp*), a dominant negative version of SOX18 that is known to disrupt SOX18 activity, decreased immunofluorescent staining of HMGCS1 and HMGCR in HUVECs. P values were calculated using a 2-tailed, unpaired t-test (**B**,**C**) and by a one-way ANOVA multiple comparisons test with Tukey-correction (**D**,**E**). Data show the mean ± SD. Data represent sample sizes n=4 (**B**,**C**) and n=3 (**D**,**E**).

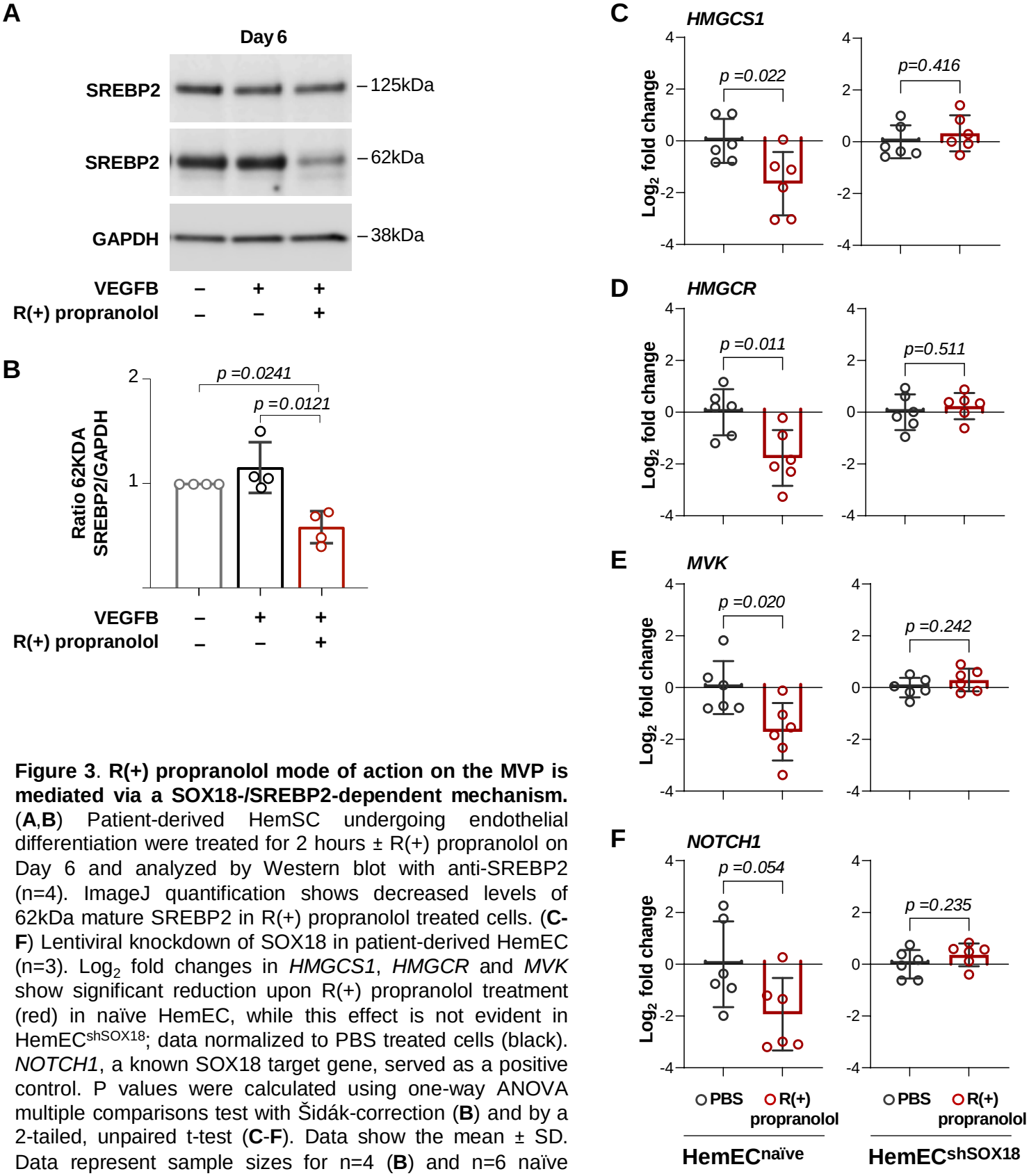

Figure 3. **R(+) propranolol mode of action on the MVP is mediated via a SOX18-/SREBP2-dependent mechanism.** (**A**,**B**) Patient-derived HemSC undergoing endothelial differentiation were treated for 2 hours ± R(+) propranolol on Day 6 and analyzed by Western blot with anti-SREBP2 (n=4). ImageJ quantification shows decreased levels of 62kDa mature SREBP2 in R(+) propranolol treated cells. (**C**-**F**) Lentiviral knockdown of SOX18 in patient-derived HemEC (n=3). Log_2 fold changes in *HMGCS1*, *HMGCR* and *MVK* show significant reduction upon R(+) propranolol treatment (red) in naïve HemEC, while this effect is not evident in $HemEC^{shSOX18}$; data normalized to PBS treated cells (black). *NOTCH1*, a known SOX18 target gene, served as a positive control. P values were calculated using one-way ANOVA multiple comparisons test with Šidák-correction (**B**) and by a 2-tailed, unpaired t-test (**C**-**F**). Data show the mean ± SD. Data represent sample sizes for n=4 (**B**) and n=6 naïve HemEC (denoted as HemEC 133,150,171) and n=6 $HemEC^{shSOX18}$ with knockdown of SOX18 performed twice in each HemEC line (efficiency >70%) in (**C**-**F**).

Figure 3

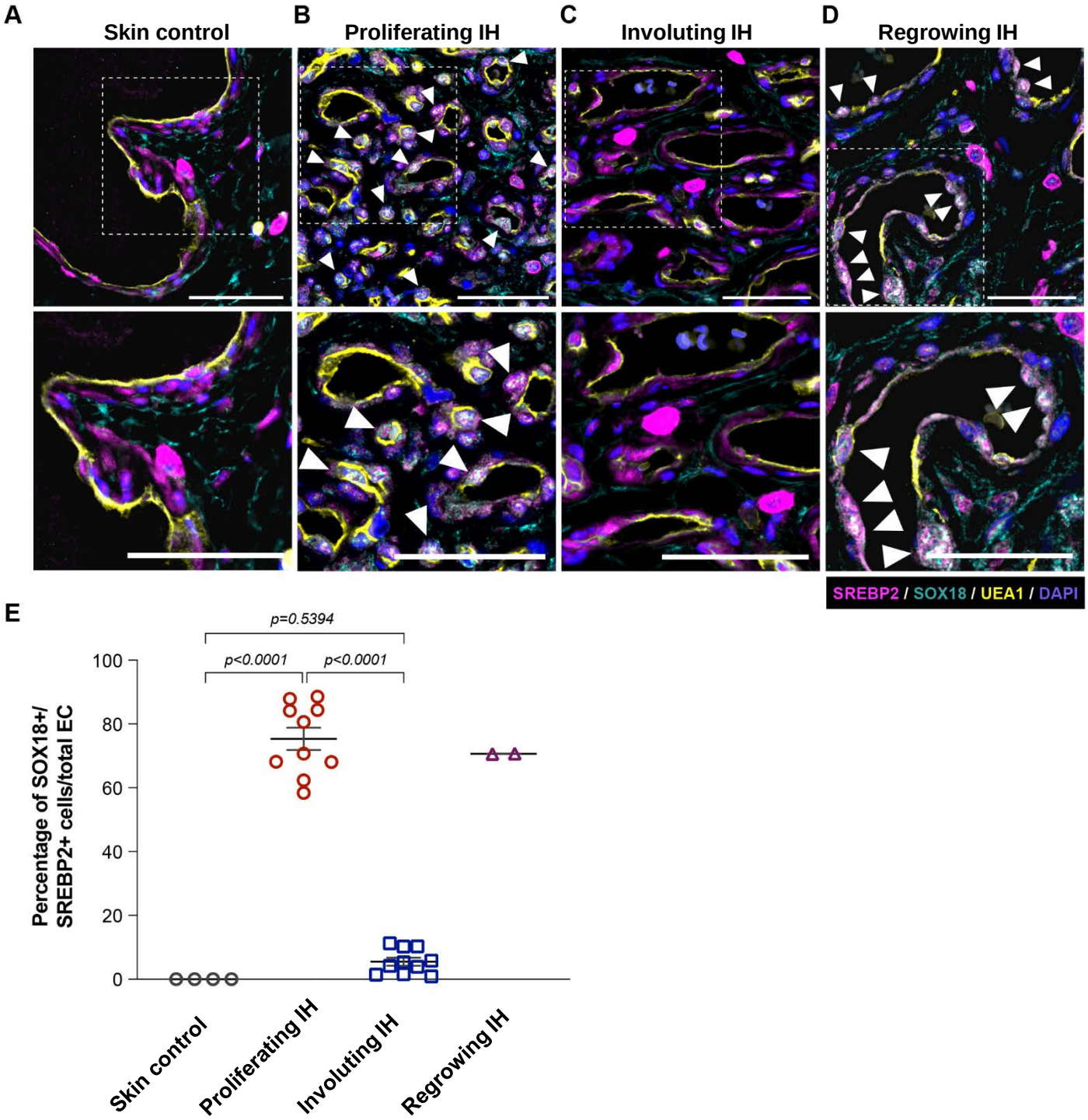

Figure 4. **Nuclear co-localization of SOX18 and SREBP2 in proliferating phase and regrowing IH indicate active MVP.** (**A**-**D**) Human age-matched skin, proliferating IH, involuting IH and regrowing IH stained for SREBP2 (magenta), SOX18 (cyan), and the human EC-specific lectin UEA1 (yellow). Cell nuclei are stained with DAPI (blue). $SOX18^{+}/SREBP2^{+}$ double positive cell nuclei (arrowheads) are significantly more abundant in proliferating phase and appear increased in regrowing compared to involuting phase IH and age-matched skin controls, as quantified in (**E**). P values were calculated using one-way ANOVA with Šidák-correction. Data show the mean ± SD. Data represent sample sizes for n=4 age-matched skin controls, n= 10 each for proliferating and involuting phase IH, and n=2 for regrowing IH. Scale bars 50 µm.

Figure 4

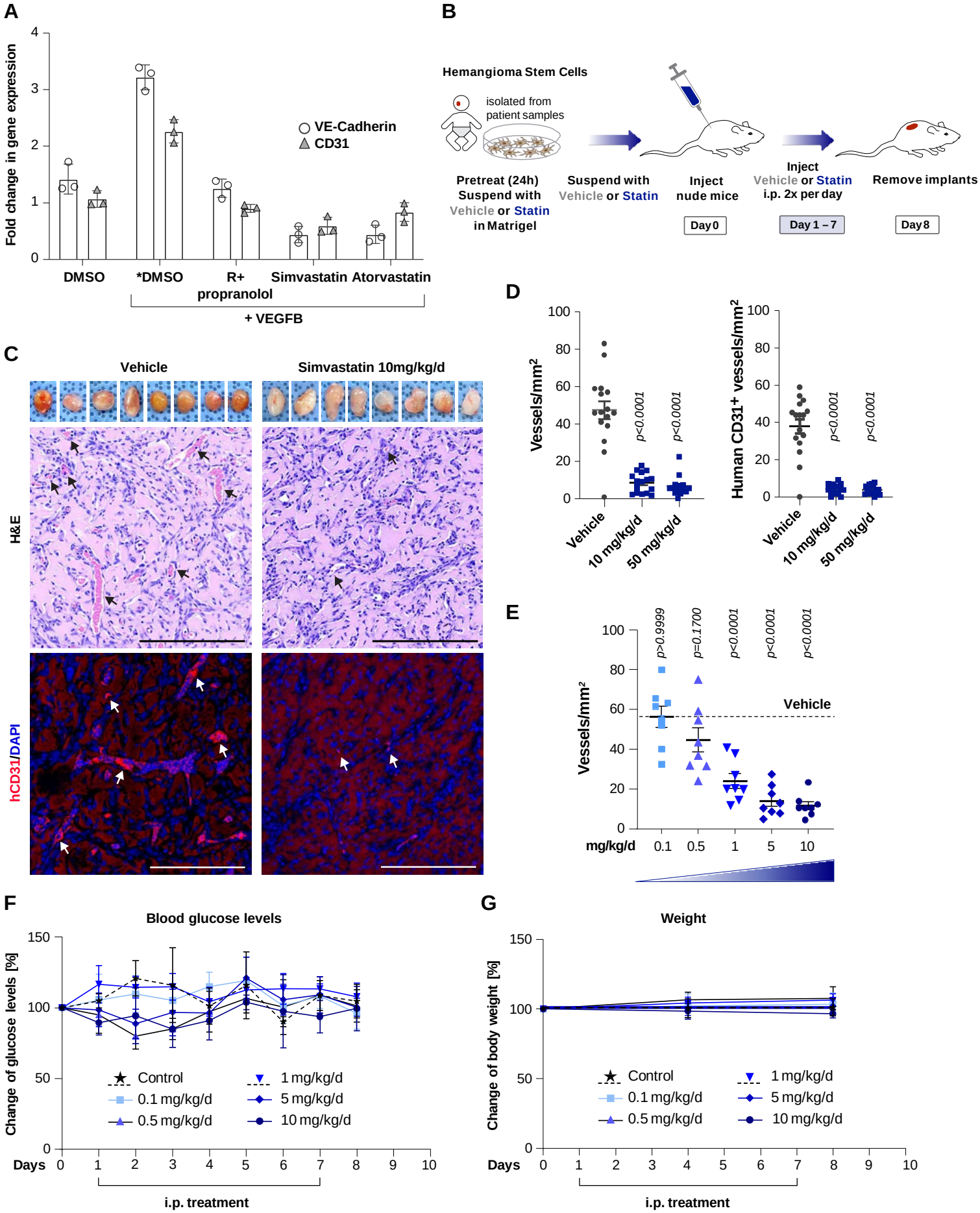
A
Fold change in gene expression
VE-Cadherin
CD31
DMSO
*DMSO
R+ propranolol
Simvastatin
Atorvastatin
+ VEGFB
B
Hemangioma Stem Cells
isolated from patient samples
Pretreat (24h) Suspend with Vehicle or Statin in Matrigel
Suspend with Vehicle or Statin
Inject nude mice
Day 0
Inject Vehicle or Statin i.p. 2x per day
Day 1 – 7
Remove implants
Day 8
C
Vehicle
Simvastatin 10mg/kg/d
H&E
hCD31/DAPI
D
Vessels/mm²
Human CD31⁺ vessels/mm²
p<0.0001
Vehicle
10 mg/kg/d
50 mg/kg/d
E
Vessels/mm²
p>0.9999
p=0.1700
p<0.0001
Vehicle
mg/kg/d
0.1
0.5
1
5
10
F
Blood glucose levels
Change of glucose levels [%]
Control
0.1 mg/kg/d
0.5 mg/kg/d
1 mg/kg/d
5 mg/kg/d
10 mg/kg/d
Days
i.p. treatment
G
Weight
Change of body weight [%]
Control
0.1 mg/kg/d
0.5 mg/kg/d
1 mg/kg/d
5 mg/kg/d
10 mg/kg/d
Days
i.p. treatment

Figure 5

Figure 5. Statins inhibits HemSC endothelial differentiation and blood vessel formation in a xenograft model of IH. (**A**) Simvastatin (1 μM) and atorvastatin (0.1 μM) inhibited VEGF-B induced endothelial differentiation of HemSC (n=3) in vitro as indicated by reduced mRNA levels of EC markers VE-Cadherin and CD31 over the course of 6 days of treatment. R(+) propranolol (20 μM) served as a positive control. P values shown in Supplemental Table S5.2) (**B**) Schematic of IH xenograft model. Patient-derived HemSC (n=4) were pre-treated with 5 μM simvastatin or vehicle (0.005% DMSO), suspended in Matrigel with 2.5 μM simvastatin or vehicle (0.0025% DMSO), and injected subcutaneously into nude mice, with 2 implants/mouse. Mice were treated with 0.1 - 50 mg/kg/d simvastatin and vehicle (max. 2.3% DMSO/dose) twice a day via intraperitoneal injections. (**C**) Matrigel implants harvested after 7 days of treatment are shown in the top panel. H&E staining indicates reduction of blood vessels in simvastatin treated compared to control mice (middle panels). Anti-human CD31 staining (red) confirmed reduced human vessel formation in simvastatin-treated mice compared to controls (bottom panels). Cell nuclei were stained with DAPI (blue). Scale bars 100 μm. (**D**) Quantification of vessels/mm^2 in the H&E-stained sections (left) and human CD31$^+$ vessels/mm^2 (right) show a significant reduction in vessel density in the implants of simvastatin-treated mice compared to control mice. (**E**) Dose response to simvastatin indicates significant inhibition of vessel formation as of 1 mg/kg/d. (**F**,**G**) Blood glucose levels and body weight of mice were unaffected in both simvastatin-treated and control mice. P values were calculated using one-way ANOVA multiple comparisons test with Tukey-correction (**A**,**D**), one-way ANOVA multiple comparisons test with Dunnett-correction (**E**), and two-way ANOVA multiple comparisons test with Dunnett-correction (**F**). Data are shown as ± SD. Data were collected for 2 implants in each mouse, leading to an observation sample size of n=24 for vehicle (combined), n=14 for 10 mg/kg/d, and n=16 for 50 mg/kg/d simvastatin (**D**) as well as in the dose response n=10 for vehicle, n=10 for 10 mg/kg/d, n=10 for 5 mg/kg/, n=10 for 1 mg/kg/d, n=10 for 0.5 mg/kg/d, and n=10 for 0.1 mg/kg/d simvastatin (**E**).

Table 1: Overview of patient cells and tissues used throughout the study

Sample ID	Gender	Age at resection	Figure
Proliferating IH (<1 year)			
P-150	M	3m	1, 3, 4, 5
P-147	M	3m	4, 5
P-138	F	3m	4
P-133	M	3m	4, 5
P-171	F	4m	1, 3, 4, 5
P-165	F	4m	1, 3, 5
P-168	F	5m	4
P-125	F	5m	1, 4
P-167	F	7m	1, 4
P-149	F	7m	1, 3, 4, 5
Involuting IH (>1 year)			
I-69	F	1y 1m	4
I-79	F	1y 6m	4
I-71	F	2y 1m	4
I-85	M	2y 2m	4
I-99	M	2y 6m	4
I-84	M	2y 6m	4
I-78	M	2y 6m	4
I-67	M	2y 6m	4
I-81	F	2y 11m	4
I-68	F	2y 11m	4
Rebounding IH			
R-1	F	6y 4m	4
R-2	F	9y 6m	4
Skin Controls			
C-1	F	8m	4
C-2	M	1y	4
C-3	M	3y 7m	4
C-4	M	5y 4m	4

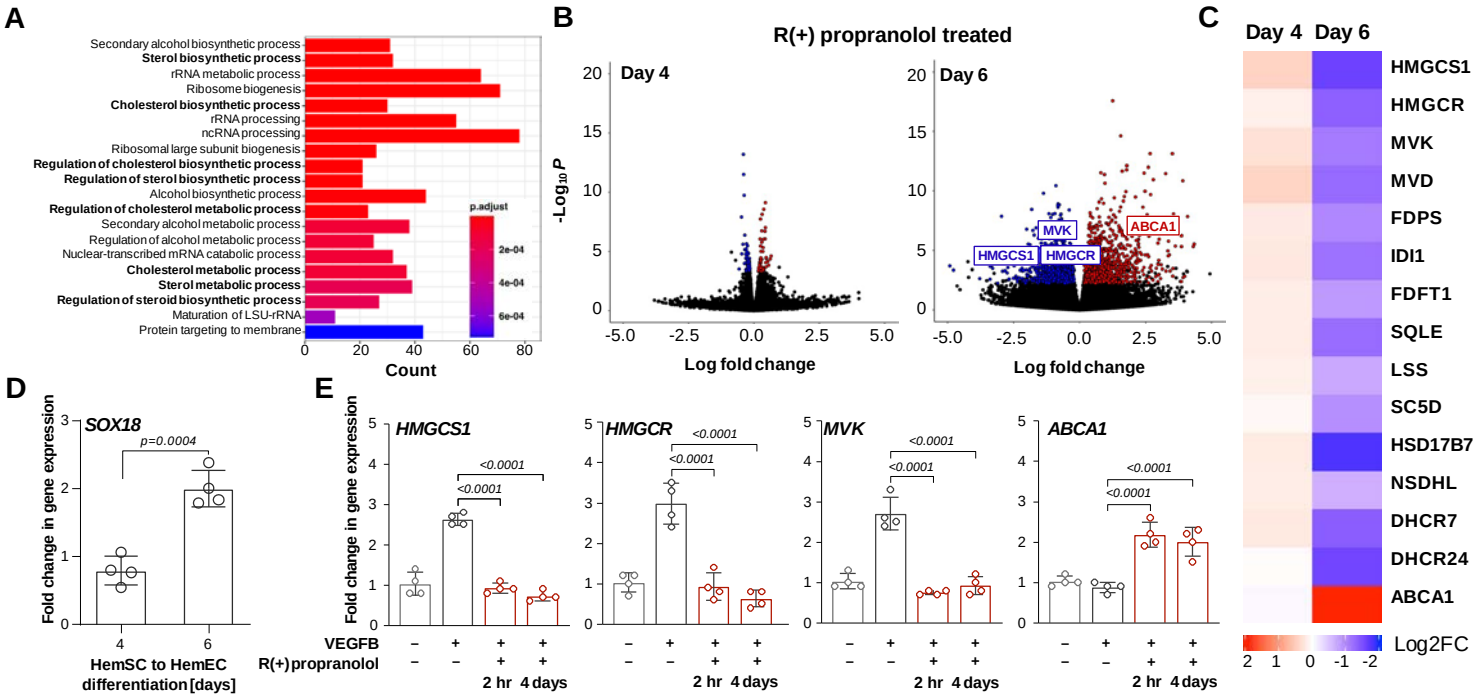

Figure 1. R(+) propranolol reduces MVP transcripts in IH -derived HemSC undergoing endothelial differentiation. (**A**) Gene ontology analysis of the subontology *biological processes* of bulk RNA-seq data set from IH-derived HemSC (n=6). (**B**) Volcano plots show an increase in differentially expressed genes on Day 6 compared to Day 4 of HemSC to endothelial differentiation. (**C**) Heat map with MVP gene transcripts at Day 4 and Day 6 as well as ABCA1 – a negative regulator of the MVP transcription factor SREBP2**.** (**D**) SOX18 measured by qPCR is significantly increased on Day 6 compared to Day 4 (n=3). (**E**) HemSC induced to undergo endothelial differentiation were treated with R+ propranolol for 2 hours on Day 6, or from Day 2-6, i.e., 4-day treatment. qPCR analyses for three MVP genes - *HMGCS1*, *HMGCR*, *MVK,* as well as *ABCA1,* a negative regulator of the MVP transcription factor SREBP2 (n=4). P values were calculated using a 2-tailed, unpaired t-test (**D**) and by a one-way ANOVA multiple comparisons test with Šidák-correction (**E**). Data show the mean ± SD. Data represent sample sizes n=4 (**D**,**E**).

Figure 1

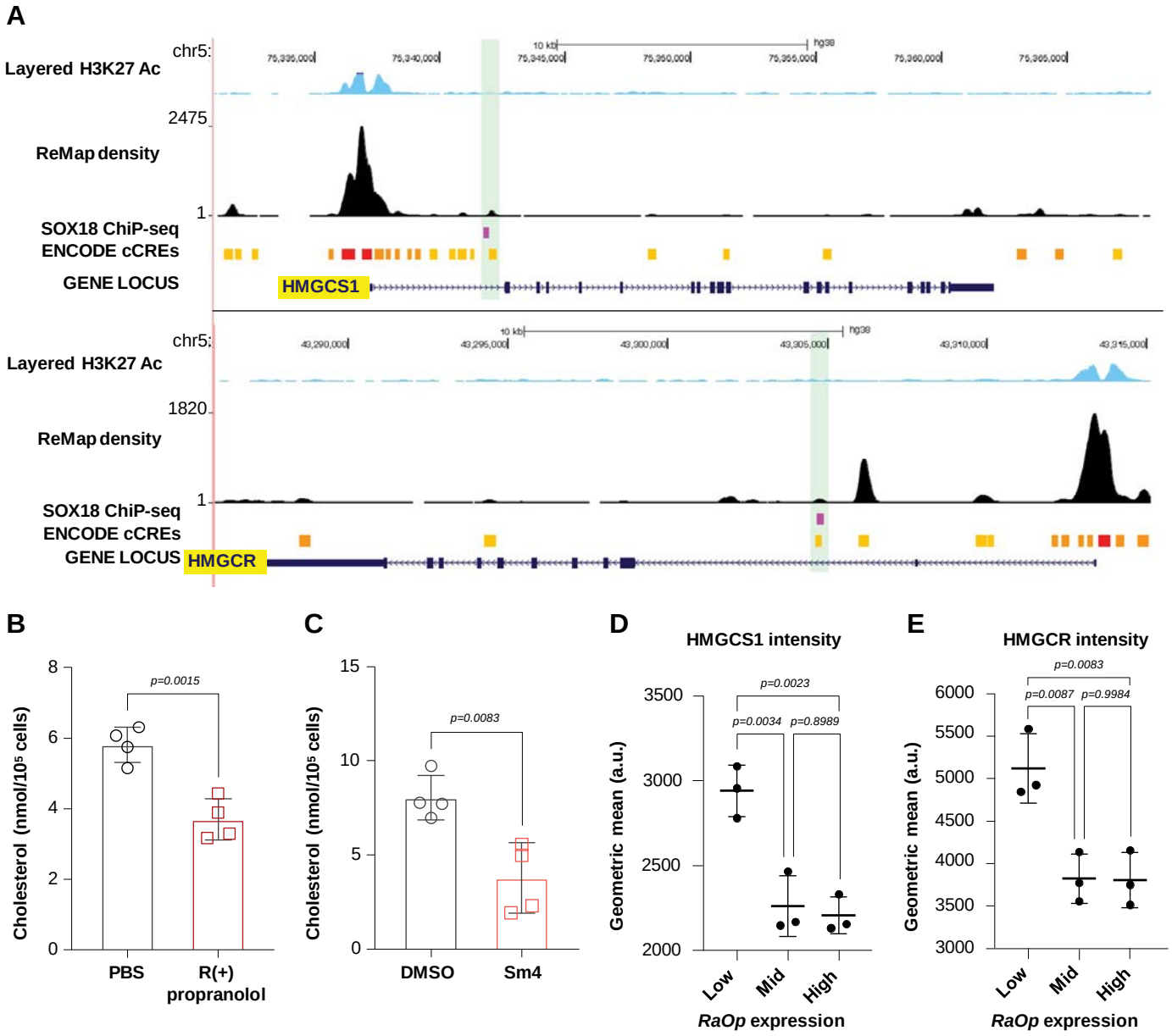

Figure 2. **SOX18 regulates the MVP in endothelial cells.** (**A**) ChIP-Seq dataset in HUVEC demonstrates SOX18 binding sites within the *HMGCS1* and *HMGCR* gene loci which correspond with ENCODE candidate cis-regulatory elements. (**B**,**C**) A functional role for SOX18 in cholesterol biosynthesis was tested by pharmacological disruption of SOX18 activity with R+ propranolol or the SOX18 inhibitor Sm4. HUVECs were cholesterol depleted by incubation with methyl beta-cyclodextrin (MBCD) for 16 hours, followed by treatment ± R(+) propranolol or ± Sm4 for 16 hours each. Endogenous cholesterol levels were measured by mass spectrometry. (**D**,**E**) Overexpression of Ragged Opossum (*RaOp*), a dominant negative version of SOX18 that is known to disrupt SOX18 activity, decreased immunofluorescent staining of HMGCS1 and HMGCR in HUVECs. P values were calculated using a 2-tailed, unpaired t-test (**B**,**C**) and by a one-way ANOVA multiple comparisons test with Tukey-correction (**D**,**E**). Data show the mean ± SD. Data represent sample sizes n=4 (**B**,**C**) and n=3 (**D**,**E**).

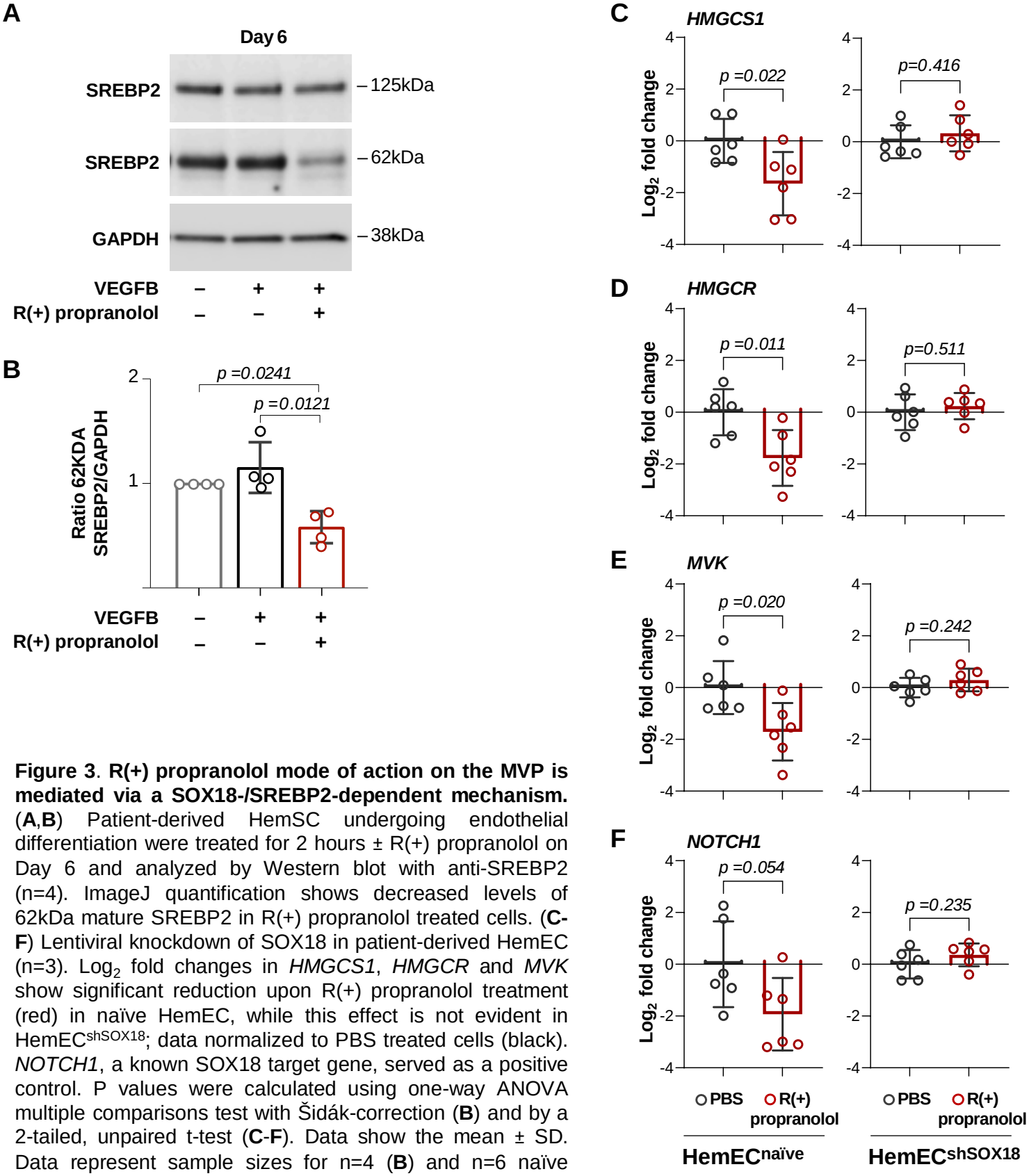

Figure 3. **R(+) propranolol mode of action on the MVP is mediated via a SOX18-/SREBP2-dependent mechanism.** (**A**,**B**) Patient-derived HemSC undergoing endothelial differentiation were treated for 2 hours ± R(+) propranolol on Day 6 and analyzed by Western blot with anti-SREBP2 (n=4). ImageJ quantification shows decreased levels of 62kDa mature SREBP2 in R(+) propranolol treated cells. (**C**-**F**) Lentiviral knockdown of SOX18 in patient-derived HemEC (n=3). Log_2 fold changes in *HMGCS1*, *HMGCR* and *MVK* show significant reduction upon R(+) propranolol treatment (red) in naïve HemEC, while this effect is not evident in $HemEC^{shSOX18}$; data normalized to PBS treated cells (black). *NOTCH1*, a known SOX18 target gene, served as a positive control. P values were calculated using one-way ANOVA multiple comparisons test with Šidák-correction (**B**) and by a 2-tailed, unpaired t-test (**C**-**F**). Data show the mean ± SD. Data represent sample sizes for n=4 (**B**) and n=6 naïve HemEC (denoted as HemEC 133,150,171) and n=6 $HemEC^{shSOX18}$ with knockdown of SOX18 performed twice in each HemEC line (efficiency >70%) in (**C**-**F**).

Figure 3

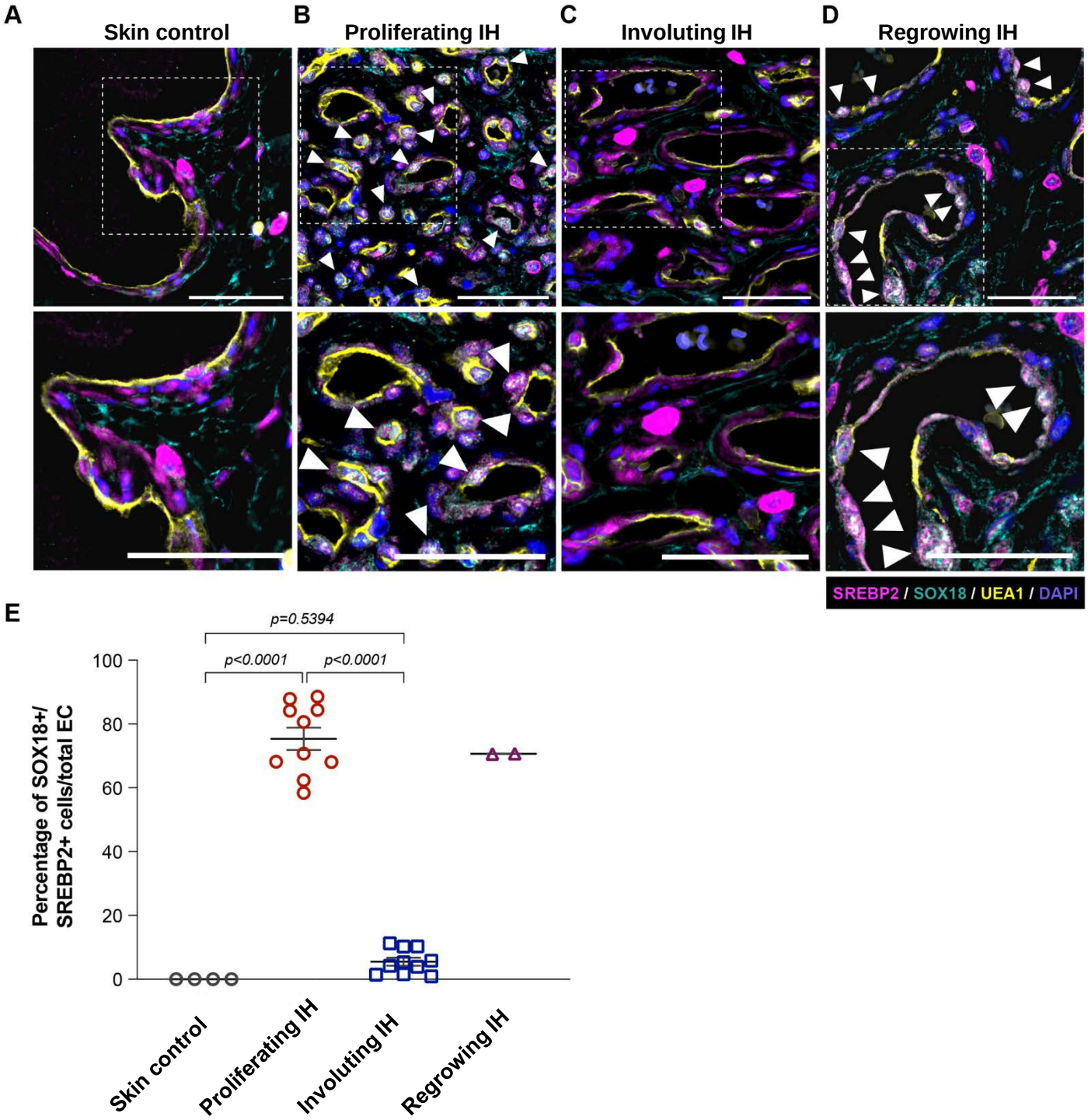

Figure 4. **Nuclear co-localization of SOX18 and SREBP2 in proliferating phase and regrowing IH indicate active MVP.** (**A**-**D**) Human age-matched skin, proliferating IH, involuting IH and regrowing IH stained for SREBP2 (magenta), SOX18 (cyan), and the human EC-specific lectin UEA1 (yellow). Cell nuclei are stained with DAPI (blue). $SOX18^{+}/SREBP2^{+}$ double positive cell nuclei (arrowheads) are significantly more abundant in proliferating phase and appear increased in regrowing compared to involuting phase IH and age-matched skin controls, as quantified in (**E**). P values were calculated using one-way ANOVA with Šidák-correction. Data show the mean ± SD. Data represent sample sizes for n=4 age-matched skin controls, n= 10 each for proliferating and involuting phase IH, and n=2 for regrowing IH. Scale bars 50 µm.

Figure 4

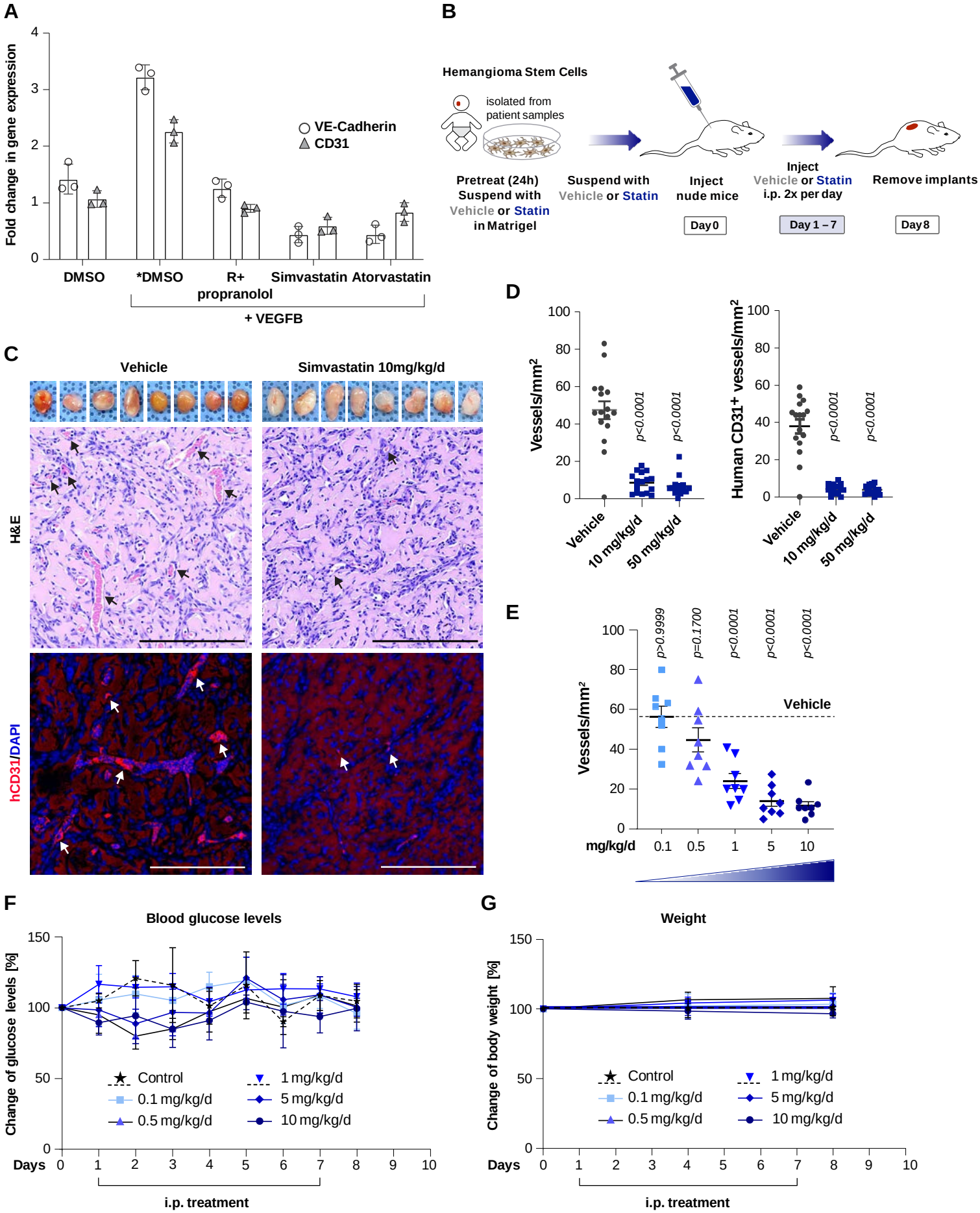
A
Fold change in gene expression
VE-Cadherin
CD31
DMSO
*DMSO
R+ propranolol
Simvastatin
Atorvastatin
+ VEGFB
B
Hemangioma Stem Cells
isolated from patient samples
Pretreat (24h) Suspend with Vehicle or Statin in Matrigel
Suspend with Vehicle or Statin
Inject nude mice
Day 0
Inject Vehicle or Statin i.p. 2x per day
Day 1 – 7
Remove implants
Day 8
C
Vehicle
Simvastatin 10mg/kg/d
H&E
hCD31/DAPI
D
Vessels/mm²
Human CD31⁺ vessels/mm²
p<0.0001
Vehicle
10 mg/kg/d
50 mg/kg/d
E
Vessels/mm²
p>0.9999
p=0.1700
p<0.0001
Vehicle
mg/kg/d
0.1
0.5
1
5
10
F
Blood glucose levels
Change of glucose levels [%]
Control
0.1 mg/kg/d
0.5 mg/kg/d
1 mg/kg/d
5 mg/kg/d
10 mg/kg/d
Days
i.p. treatment
G
Weight
Change of body weight [%]
Control
0.1 mg/kg/d
0.5 mg/kg/d
1 mg/kg/d
5 mg/kg/d
10 mg/kg/d
Days
i.p. treatment

Figure 5

Figure 5. Statins inhibits HemSC endothelial differentiation and blood vessel formation in a xenograft model of IH. (**A**) Simvastatin (1 μM) and atorvastatin (0.1 μM) inhibited VEGF-B induced endothelial differentiation of HemSC (n=3) in vitro as indicated by reduced mRNA levels of EC markers VE-Cadherin and CD31 over the course of 6 days of treatment. R(+) propranolol (20 μM) served as a positive control. P values shown in Supplemental Table S5.2) (**B**) Schematic of IH xenograft model. Patient-derived HemSC (n=4) were pre-treated with 5 μM simvastatin or vehicle (0.005% DMSO), suspended in Matrigel with 2.5 μM simvastatin or vehicle (0.0025% DMSO), and injected subcutaneously into nude mice, with 2 implants/mouse. Mice were treated with 0.1 - 50 mg/kg/d simvastatin and vehicle (max. 2.3% DMSO/dose) twice a day via intraperitoneal injections. (**C**) Matrigel implants harvested after 7 days of treatment are shown in the top panel. H&E staining indicates reduction of blood vessels in simvastatin treated compared to control mice (middle panels). Anti-human CD31 staining (red) confirmed reduced human vessel formation in simvastatin-treated mice compared to controls (bottom panels). Cell nuclei were stained with DAPI (blue). Scale bars 100 μm. (**D**) Quantification of vessels/mm^2 in the H&E-stained sections (left) and human CD31$^+$ vessels/mm^2 (right) show a significant reduction in vessel density in the implants of simvastatin-treated mice compared to control mice. (**E**) Dose response to simvastatin indicates significant inhibition of vessel formation as of 1 mg/kg/d. (**F**,**G**) Blood glucose levels and body weight of mice were unaffected in both simvastatin-treated and control mice. P values were calculated using one-way ANOVA multiple comparisons test with Tukey-correction (**A**,**D**), one-way ANOVA multiple comparisons test with Dunnett-correction (**E**), and two-way ANOVA multiple comparisons test with Dunnett-correction (**F**). Data are shown as ± SD. Data were collected for 2 implants in each mouse, leading to an observation sample size of n=24 for vehicle (combined), n=14 for 10 mg/kg/d, and n=16 for 50 mg/kg/d simvastatin (**D**) as well as in the dose response n=10 for vehicle, n=10 for 10 mg/kg/d, n=10 for 5 mg/kg/, n=10 for 1 mg/kg/d, n=10 for 0.5 mg/kg/d, and n=10 for 0.1 mg/kg/d simvastatin (**E**).